UBMEJEN
UNIVERSITIÄHTA

On the operation of light-emitting electrochemical cells

Mattias Lindh

Department of Physics

Umeå 2019

Dissertation for PhD
ISBN: 978-91-7855-000-5
Cover: $I_e(\theta, \lambda)$ of a detuned LEC
Electronic version available at: `http://umu.diva-portal.org/`
Printed by: CityPrint i Norr AB
Umeå, Sweden 2019

“The mountains are calling and I must go.”
—John Muir

Abstract

WE ARE IN THE MIDST OF A TECHNOLOGICAL REVOLUTION that permeates nearly all human activities; artificial light is one of the most visible contributors in this societal change. If more efficient, green, and versatile light sources can be developed, they might improve the life of millions of people around the world while causing minimal damage to our climate and environment. The unique operational mechanism of the light-emitting electrochemical cell (LEC) makes it an ideal fit for some unconventional and emerging uses of light, in for example medicine and security.

By exploiting this operational mechanism, in which mobile ions enable electrochemical doping of a luminescent polymer, we have designed and fabricated new bilayer LEC architectures. The bilayer LEC features patterned light emission that is easily adjustable during fabrication, and that can be configured to suit new applications of light. Given the light-emitting nature of the LEC, it is somewhat surprising that the optical understanding of its operation is rather limited. To fill this knowledge gap, we investigate how the optical properties of the luminescent polymer respond to electrochemical doping. We find that the complex-refractive index spectrum in the active layer of an LEC, as a direct result of the doping, varies in both space and time. The thin-film structure of an LEC implies that computational predictions of its luminous output need to consider internal reflections and interference. Finally, we implement a doping-dependent optical thin-film simulation model. It enables us to precisely replicate the experimental luminance and angle-dependent emission spectrum for a range of LECs with different thicknesses. Using the model we can also identify and quantify many of the different optical loss mechanisms in LECs, which has not previously been done. The insights that we have collected on the path towards our present model will be useful for computational determination of device parameters that are otherwise difficult to acquire.

The improved understanding of the optical operation of LECs is important for the maturation of the technology, as it facilitates formulation of relevant and accurate research questions. Hopefully, our results will accelerate the development of the field, so that useful products based on this technology can become available in the not too distant future.

Sammanfattning

JUST NU PÅGÅR EN TEKNOLOGISK REVOLUTION som genomsyrar nära nog alla samhällsfunktioner, och där artificiellt ljus har en påfallande viktig roll. Nya ljuskällor, som är mer miljövänliga, effektiva och mångsidiga, skulle kunna förbättra livskvaliten för miljoner människor över hela världen, utan att för den skull skapa problem för vår miljö och vårt klimat. Den ljusemitterande elektrokemiska cellen (LEC) är en teknik som fungerar på ett unikt sätt. Det gör att den är lämplig för nya och okonventionella användningsområden av ljus, exempelvis inom medicin och säkerhetsprodukter.

Vi har kunnat designa och tillverka en ny sorts dubbellagers-LEC genom att utnyttja den interna funktionen i en LEC. Den innebär att rörliga joner möjliggör elektrokemiska oxidations- och reduktionsprocesser (dopning) av en lysande polymer. En dubbellagers-LEC lyser i mönster som enkelt kan anpassas utefter önskemål, och skulle kunna användas i nya sorters ljusapplikationer. Med tanke på att en LEC är en lysande komponent är förståelsen för dess optik förvånansvärt begränsad. För att förbättra dessa kunskaper börjar vi med att undersöka hur den lysande polymerens optiska egenskaper förändras när den dopas. Vi finner att dess optiska egenskaper varierar i tid och rum i det aktiva skiktet i en LEC, som en direkt följd av dopningen. För att sedan med hjälp av de optiska egenskaperna kunna beräkna hur mängden ljus påverkas, måste vi också ta hänsyn till att ljus i tunna skikt kan reflekteras vid gränsytor och interagera med sig själv. Slutligen implementerar vi en dopningsberoende optisk beräkningsmodell för tunna skikt, och lyckas återskapa den experimentellt uppmätta luminansen och de vinkelberoende ljusspektrumen för en serie LECer med olika tjocklek. Utifrån modellen kan vi också identifiera och kvantifiera många av de olika optiska förlustkanalerna i en LEC, vilket inte gjorts tidigare. Vägen fram till den nuvarande modellen har bjudit oss på en rad insikter som gör att vi beräkningsmässigt kan uppskatta komponentegenskaper som annars skulle förbli okända, då de inte går att mäta med direkta metoder.

Den förbättrade optiska förståelsen för LEC-tekniken är viktig för forskningen inom fältet. Våra resultat kan förhoppningsvis accelerera utvecklingen mot bra och användbara produkter, så att dessa blir tillgängliga inom en inte alltför avlägsen framtid.

Contents

Publications

This thesis is based on the following publications, reprinted with permission from the publishers:

I *Inkjet printed bilayer light-emitting electrochemical cells for display and lighting applications*
E. Mattias Lindh, Andreas Sandström, and Ludvig Edman
Small, Vol. 10, no. 20, p. 4148–4153, 2014

II *Luminescent line art by direct-write patterning*
E. Mattias Lindh, Andreas Sandström, Mats Andersson, and Ludvig Edman
Light: Science & Applications, Vol. 5, id. e16050, 2016

III *On the asymmetric evolution of the optical properties of a conjugated polymer during electrochemical p- and n-type doping*
Thomas Lanz, **E. Mattias Lindh**, and Ludvig Edman
Journal of Materials Chemistry C, Vol. 5, p. 4706–4715, 2017

IV *The weak microcavity as an enabler for bright and fault-tolerant light-emitting electrochemical cells*
E. Mattias Lindh, Petter Lundberg, Thomas Lanz, Jonas Mindemark, and Ludvig Edman
Scientific Reports, Vol. 8, id. 6970, 2018

V *Optical analysis of light-emitting electrochemical cells*
E. Mattias Lindh, Petter Lundberg, Thomas Lanz, and Ludvig Edman
Submitted

Papers not included in the thesis:

Simulated productivity of conceptual, multi-headed tree planting devices
Back Tomas Ersson, Linus Jundén, **E. Mattias Lindh**, and Urban Bergsten
International Journal of Forest Engineering, Vol. 25, No. 3, p. 201–213, 2014

Toward efficient and metal-free emissive devices: A solution-processed host-guest light-emitting electrochemical cell featuring thermally activated delayed fluorescence
Petter Lundberg, **E. Mattias Lindh**, Shi Tang, and Ludvig Edman
ACS Applied Materials & Interfaces, Vol. 9, p. 28810–28816, 2017

Challenging conventional wisdom: Finding high-performance electrodes for light-emitting electrochemical cells
Jin Xu, Andreas Sandström, **E. Mattias Lindh**, Wei Yang, Shi Tang, and Ludvig Edman
ACS Applied Materials & Interfaces, Vol. 10, p. 33380–33389, 2018

Patent applications:

Light-emitting electrochemical cell and method of its manufacture
Andreas Sandström, **E. Mattias Lindh**, and Ludvig Edman
PCT patent no. EP2014/055868, Filing date: 24th March 2014

Preface

SCIENCE is in some sense a religion: it only makes sense if you believe in it. But unlike most other religions that I know of, science is inherently dynamic and built on change. When a new finding is reported, the scientific community typically rejects, questions, refines, or embraces it in an iterative process. This has been the course and evolution of knowledge since the time of Plato and Aristotle. Generations of hard-working scientists have in this way laid out the foundations for safe housing, food production, healthcare, education, and other prerequisites of the good life we enjoy today. But isn't it ironic, that as science has provided conveniences, those conveniences have brought with them a fierce resistance to change? 27 years after the Earth Summit in Rio, the pace is still painfully, and recklessly, slow.[1, 2] As a committed believer in science, I just cannot accept that this should be a time for "business as usual".[3]

Science somehow brought us here. To a warming climate and its aftermath. To an Earth entering Anthropocene, the new geological epoch.[4, 5] To the sixth mass extinction in the history of our planet.[6] To an ocean filled with plastic trash, and a biosphere pestered with drugs and chemicals.[7–9] But if we believe in science, and heed its united calls for action, there may be ways to recover sustainability and pass on a hospitable planet to our children: Now is the time for change.

SCIENCE — SAVE OUR SOULS.

Mattias Lindh, Ostön
January 2019

1. Introduction

PLASTIC IS OLD NEWS. For example, polystyrene, polyvinyl chloride, and polyethylene were all discovered in the 19th century.[10–12] Today, such plastic materials (or polymers, which they really are) are incredibly useful and abundant materials used in packaging, electrical and thermal insulation, and as easily mouldable (even printable!) manufacturing materials, among many other things. But in the 1970s, Heeger, MacDiarmid, Shirakawa, and co-workers, showed that polymers are also fantastic, high-tech materials, and they were awarded the Nobel Prize in chemistry in the year 2000. They had discovered that some properly treated (conjugated) polymers can become electrically conducting, with an almost metallic conductivity.[13, 14] The treatment involved exposure to a halogen gas (e.g., chlorine, bromine or iodine) that oxidized the materials and altered the density of electronic charges. The polymer had become chemically *doped*, and the electric conductivity improved drastically.[15, 16] But remarkably, some of these semiconducting conjugated polymers can also be luminescent, because they have an energy gap between its ground state and its excited state that correspond to the energy of visible light.[17] The optical, electronic, and mechanical properties of semiconducting polymers combined, and the innumerable chemical structures that can be varied during their synthesis, makes them a unique class of materials with a world of possible applications.

Electrically conductive polymers can be used in for example anti-static films, smart windows with adjustable transmittance, organic photovoltaic cells, and organic light-emitting diodes.[18–20] Today, organic light-emitting diodes are found on the market in pixelated television and smartphone screens, and they can be designed for automotive and everyday lighting. But the special properties of polymeric light-emitting materials may also allow for new and untraditional uses of light in e.g., light-emitting band aids and validation of important or valuable documents. The light-emitting electrochemical cell (LEC) technology is a strong candidate for such unconventional and emergent uses of light, because they are comparatively robust and can be made on a wide variety of substrates such as paper and textile,[21–24] and using simple, potentially low-cost and up-scalable fabrication processes like roll- and spray

coating.[25–30] LECs relate closely to the findings of Heeger, MacDiarmid, and Shirakawa, because they utilize doping of conjugated polymers for the generation of light.[31, 32] The doping takes place in a single thin and solid "active-layer" film, in which a salt has been blended with a luminescent polymer and electronic charges are supplied from two electrodes. During operation, electrochemical reduction and oxidation reactions (doping) give rise to a multilayer structure that takes care of the essential tasks for a light-emitting device: charge injection, charge transport and light generation.[33]

Because of the *in-situ* development of an electrochemically doped multilayer structure, it is difficult to formulate simple and robust models that capture the characteristic behaviour of LEC operation; many of the internal processes depend on each other and change in both space and time.[33–35] With this in mind, it is natural that much of the progress has been achieved through large experimental efforts.[26, 36–38] Nevertheless, models are important to understand our experimental observations, and for asking the most effective research questions during design of future experiments. To accelerate and direct future research, we therefore need a comprehensive model of LEC-operation. Qualitative models for how an LEC work electrically—up to the point at which light has been generated in the device—have been developed and verified, but optical models that can quantify the amount of emitted light are lacking.[39] Efforts to adopt knowledge from neighbouring research fields have begun, however, while the electrical model suggest that electrochemical doping strongly affects the light emission, existing optical models so far do not consider these interactions.[39–41]

We fill this gap by including the optical effects of electrochemical doping in our optical operation model of an LEC. A future coupling between an electrical and an optical model that both take doping into account will be a demanding task, but it will likely also be rewarding. More experimental data, and a detailed better understanding of what those data mean, will hopefully accelerate the research towards useful and sustainable LECs that can improve the quality of life for people, while causing minimal damage to our precious planet and society.

In this thesis I summarize and elaborate on some of our findings and some of the insights that I have acquired during my years as a PhD student. To set a common ground and give a head start to the reader, I describe some common fabrication and characterization techniques, and give a brief explanation of an operation model of LECs (seen from an electrical perspective) in chapter 2. The special operation mechanism can be exploited in a new device architecture—the bilayer sandwich LEC—and in chapter 3 I present two different incarnations. Both of them result in patterned emission, and have features that visualize the strong effects on light-emission that electrochemical doping can have. In chapter 4 we quantify how the optical properties (the refractive-index and

extinction-coefficient spectra) of a luminescent polymer are affected by electrochemical doping, and in chapter 5 I present simulation results from using these optical-property data in a realistic *optical* operation model of LECs matched to experimental data. The model quantifies the distribution of optical loss channels which I discuss in chapter 6. Chapter 7 concludes the thesis by summarizing our main findings, and putting them in the perspective of (my view of) the current state of the LEC-research field, and what lies ahead.

Dealing with research in general, and light-emitting electrochemical cells in particular, requires certain resilience and a non-negligible amount of patience. To get into a nice and soft reading mood, I suggest that you pour yourself a bold cup of pitch-black organic coffee, orient yourself into a comfortable position, and follow along a path beaten by the warriors of light.[42]

2. Basics of the light-emitting electrochemical cell

THE LEC FEATURES AN ACTIVE LAYER containing a luminescent polymer (organic semiconducting small molecules can also be used) positioned in between two electrodes: a positive anode and a negative cathode. During operation, holes (i.e. the absence of electrons) are injected into the luminescent polymer from the anode, and electrons are injected from the cathode. Light is generated when they meet. To improve the charge injection and transport, an electrolyte (i.e. mobile ions) is added in the form of a salt. Since ions are typically polar, and the organic emissive material typically non-polar, an ion-dissolving and -transporting material that blends well with the emissive material is needed. Together, the luminescent polymer, the ion-transporting material, and the salt, constitute the active layer.

2.1 General structure

In practical area-emitting LECs, at least one of the two electrodes needs to be transparent for the generated light to escape into air. The substrate, electrodes, and the active layer are stratified to form a stack or "sandwich", as shown in in Fig. 2.1a and b. This sandwich structure was used for the LECs in paper **IV** and **V**. The active layer contained a phenyl-substituted poly(*para*-phenylenevinylene) co-polymer (commonly termed "Super Yellow") as the luminescent polymer, an *n*-octyl carbonate-capped trimethylolpropane ethoxylate oligomer (TMPE-OC) as the ion-transporting material, and the alkali salt lithium trifluoromethane sulfonate ($LiCF_3SO_3$) to provide the mobile ions. Semi-transparent indium-tin oxide (ITO) on a glass substrate served as an anode, and reflective aluminium served as a cathode. The chemical structures of the materials are presented in Fig. 2.1c, together with the structure of an alternative polymeric ion-dissolving material, poly(ethylene oxide) (PEO).[i]

[i] PEO and KCF_3SO_3 was used instead of the TMPE-OC and $LiCF_3SO_3$ in papers **I** and **II**.

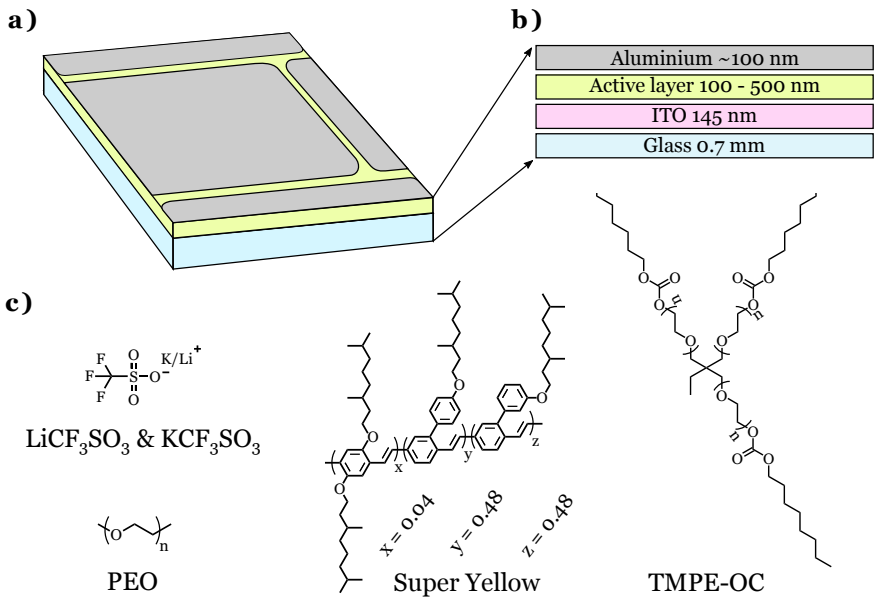

Figure 2.1: General LEC structure and materials. **a**) The sandwich device structure. **b**) An exploded view and some typical thicknesses of the layers. **c**) The chemical structures of the alkali salts $LiCF_3SO_3$ and KCF_3SO_3, the ion-dissolving and ion-transporting materials PEO and TMPE-OC, and the luminescent conjugated copolymer Super Yellow.

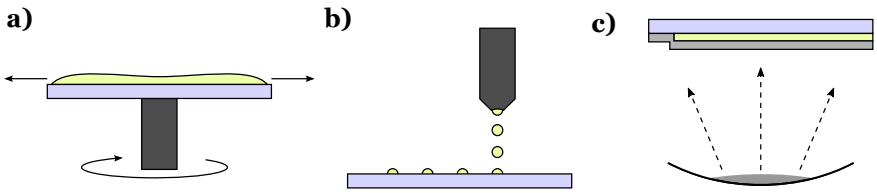

Figure 2.2: Fabrication techniques. **a)** The spincoating procedure where the rotation of the sample distributes and expels the deposited ink and leaves a thin homogeneous film on the substrate. **b)** Inkjet deposition of separated ink droplets whose position can be controlled by the software of the inkjet printer. **c)** Physical vapour deposition where a metal pellet (e.g., aluminium) is heated until it starts to evaporate, and where the vapour deposits on the substrate.

2.2 Fabrication techniques

The LECs in this thesis are all fabricated on top of commercially available (high quality) glass substrates with a thickness of 0.7 mm and predeposited 145 nm thick ITO. The active layer and the reflective metal cathode are deposited in-house using three common techniques: spin coating, inkjet printing, and physical vapour deposition, as sketched in Fig. 2.2a–c. The materials in the active layer can be dissolved in organic solvents (e.g., cyclohexanone and toluene) with suitable solubility parameters to form inks. These inks can be mixed to a composite ink that contains all the ingredients of the active layer. In the spincoating process, the ink is deposited on top of the substrate, which is then rotated (spun) according to a number of set parameters (acceleration, rotational speed, and duration) which ideally results in a homogeneous thin film covering the substrate and anode. Remaining solvent can be removed by heating the sample on a hotplate or placing it under vacuum. If an ink has suitable viscoelastic properties it can also be deposited using a special material inkjet printer.[43] In paper **I** we use inkjet technology to get well-defined and separated droplets of PEO-based electrolyte on top of the ITO anode. Typically, material preparation and device fabrication take place in gloveboxes with inert nitrogen atmosphere and low oxygen and water content, but it can also be done in the ambient air.[ii]

A thin metal film (in these studies aluminium for the formation of a cathode) can be deposited on top of the dry organic layer(s) through the process of physical vapour deposition. A metal pellet is placed in a tungsten container that is heated through resistive heating (like the filament in a classic light bulb) until the pellet melts and starts to evaporate. As the metal vapour impinges on a surface (e.g., the active layer) it deposits and forms a solid metal film. The

[ii] During operation, the active layer of an LEC is sensitive to oxygen and water. The easy way to keep these elements out of the device, is to never let them in during fabrication.

nitrogen gas in the evaporation chamber is evacuated before deposition, and especially in the case of aluminium (which is quite reactive and easily forms non-conductive oxides), a high vacuum environment is required to get a final thin film of pure aluminium with high quality.[44] The thickness of the evaporated film can be monitored as it forms, in the Å–µm range, by a calibrated quartz crystal oscillator. The shape of the final cathode of the device can be controlled by inserting a shadow mask between the source and the sample. In the end it is the overlap between the bottom ITO anode and the top aluminium cathode that defines the emissive area of a sandwich LEC.

2.3 Characterization techniques

Standard characterization techniques for LECs are focused on the driving (or operating) voltage (V) and current density (J), the forward-direction luminance (L, in units of cd m^{-2}), and the emission spectrum, $I_e(\lambda)$, where λ denotes the wavelength of the light. The efficiency with which an LEC turns electric current into visible light can conveniently be described by the (forward-direction) luminous current efficacy (η), which is given in units of cd A^{-1} as $\eta = L/J$.[iii] The nature of LEC operation is dynamic, which will be described in more detail in section 2.4. This implies that the electric and luminous properties vary during device operation, and for this reason the measured quantities are usually presented with respect to time.

2.3.1 Voltage, current density, and luminance transients

A source-measure unit is a power supply that we use to simultaneously supply and measure the current density and voltage of an LEC. It is typically configured in either a constant current or constant voltage mode, with the other variable allowed to vary within preset bounds. The luminance, which is a measure of how bright the emissive area looks to a human eye, can be measured with a dedicated luminance meter. However, for time-dependent measurements it is more practical to use a calibrated photodiode set-up with an integrated eye-response filter, and adjustable data-collection software such as a LabVIEW virtual instrument, see sketch in Fig. 2.3a. Example measurements of the evolving operating voltage and luminance of an LEC driven in constant current mode is shown in Fig. 2.3b.

[iii] The external quantum efficiency, defined as the number of emitted photons per 100 injected electrons (to get %), is a better measure of the efficiency, but it is more cumbersome to measure appropriately.

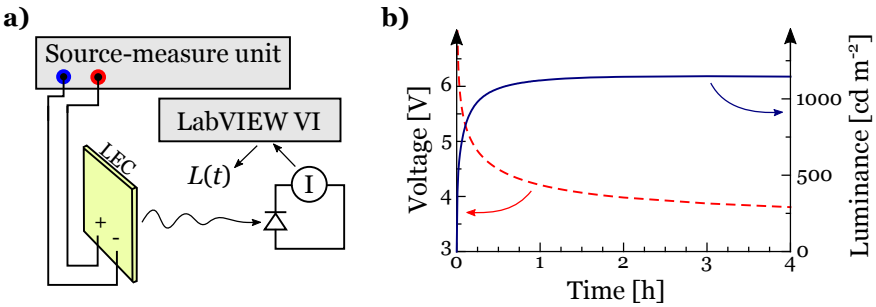

Figure 2.3: Current, voltage, and luminance measurements. **a)** A source-measure unit supplies power and measures the operating voltage and current. A photodiode connected to a LabVIEW virtual instrument monitors the emitted intensity and luminance with respect to time. **b)** A typical evolution of the operating voltage (red dashed line), and luminance (blue solid line), for a Super-Yellow based LEC during constant current density driving at 25 mA cm^{-2}.

2.3.2 Emission spectroscopy

Depending on the distribution of energetic states in the luminescent polymer, its emission spectrum and colour will vary.[45] The spectral intensity of the emission can be measured with a spectrometer, and in this work we have used CCD-array type spectrometers that allows the full emission spectrum to be captured in a single measurement (a grating distributes light with different wavelengths onto different pixels of the detector). The emission can be generated by exciting the material with light that the luminescent polymer can absorb, and this photoinduced emission is called photoluminescence. It can also be electrically induced and the emission is then called electroluminescence. Our measurement set-up collects some of the generated light with a collimating lens, and an optical fibre delivers it to the spectrometer, as depicted in Fig. 2.4a.

It is important to be aware that the "counts"-unit of the raw intensity spectrum $\left(I_c(\lambda)\right)$ from this kind of spectrometer refers to the number of accumulated electrons on each pixel of the detector. The shape of $I_c(\lambda)$ therefore depends on the wavelength sensitivity of the spectrometer. A useful and representative emission spectrum is rather given by the spectral radiant intensity ($I_e(\lambda)$, in unit of W sr^{-1} nm^{-1}). $I_e(\lambda)$ can be attained from $I_c(\lambda)$ by subtracting the dark spectrum and multiply with an instrument-specific wavelength response function. The instrument response function can in turn be gained through a reference measurement of a well-defined light source (such as a high quality halogen lamp with black-body emission). Eq. (2.1) describes the photon energy (E) of light with different wavelengths, where h is Planck's constant and c is the speed of light in vacuum. Together with $I_e(\lambda)$, Eq. (2.1) gives the spectral number of

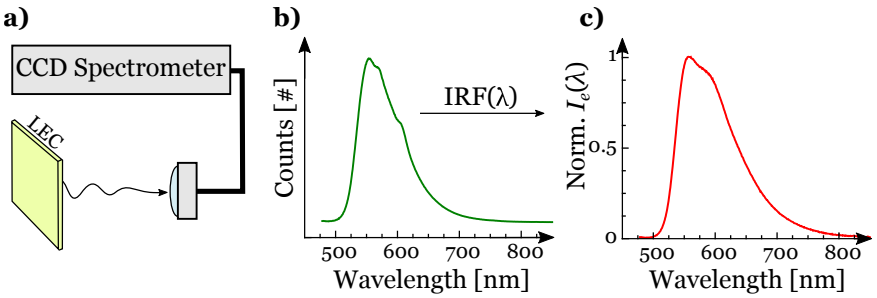

Figure 2.4: Emission spectroscopy. **a)** Sketch of the set-up for measuring the emission spectrum of a material or device. **b)** A raw luminescence intensity spectrum as obtained directly from the spectrometer, which via an instrument response function can be adjusted to a radiant intensity spectrum. **c)** The resulting radiant intensity spectrum. In this case the normalized photoluminescence of a thin Super Yellow film.

photons ($I_p(\lambda)$, in unit of $sr^{-1}\,nm^{-1}\,s^{-1}$), as described by Eq. (2.2), which is required to calculate the external quantum efficiency of a device.

$$E = \frac{hc}{\lambda} \tag{2.1}$$

$$I_p(\lambda) = \frac{\lambda \cdot I_e(\lambda)}{hc} \tag{2.2}$$

Reflection and transmission measurements, which we use in paper **III**, are performed by collecting light reflected off (or transmitted through) a sample, rather than its emission. The measured reflection- or transmission-intensity spectrum $\left(I_{R,T}(\lambda)\right)$ is of course also affected by the wavelength sensitivity of the spectrometer. To get the transmittance $\left(T(\lambda)\right)$ or reflectance $\left(R(\lambda)\right)$ of a sample, we can therefore follow the same routine as for emission, and perform a reference measurement of a sample with a well-defined reflectance (or transmittance). This procedure is described for reflectance (without explicit wavelength dependence for clarity) by Eq. (2.3).

$$R_{sample} = \left(\frac{I_{R,sample} - I_{R,dark}}{I_{R,ref} - I_{R,dark}}\right) \cdot R_{ref} \tag{2.3}$$

2.3.3 Spectroscopic goniophotometry

A more detailed characterization of the emission from LECs, which also takes the viewing-angle (θ) dependence of the emission into account, was required

for paper **IV**. For this purpose I designed and built a semi-automatic spectroscopic goniophotometer, schematically depicted in Fig. 2.5. This set-up provides all the metrics given by the methods in sections 2.3.1 and 2.3.2, and adds a few. As before, a source-measure unit is used for driving the LEC, which is mounted in a connection jig on top of a stepper motor. A LabVIEW virtual instrument controls the stepper motor via a USB-data acquisition card, and synchronizes the rotation of the LEC to a spectrometer that collects the raw emission spectrum for each specified viewing angle. Further analysis and post processing is at this stage performed in Matlab. It is notable that a carefully determined instrument response function and angle-resolved emission characterization give access to a number of additional emission metrics without using an integrating sphere.[iv] The integration can instead be performed numerically, with respect to the wavelength, the viewing angle, or both. This way, metrics like the external quantum efficiency and luminous power efficacy can be measured without assumptions regarding the angle dependence of the luminous intensity and emission spectrum (which are required if we were to use only the forward luminance and emission spectrum). To investigate the polarized contributions from the emission, a linear polarization filter can optionally be positioned in front of the collimating lens.

2.4 Electric operation

With the fabrication and characterization procedures in place, let us now look at the established *electric* operation-mechanism of the LEC in some more detail. During the early years of the millennium, the operation mechanism and the role of doping in LECs was under intense scientific debate with two seemingly incompatible models—the electrodynamic and the electrochemical—both more or less claiming to be exclusively correct.[46, 47] In 2010 van Reenen et al. finally settled the matter by presenting a unifying theory encompassing both models, with the original electrochemical model being the most representative for well-functioning and efficient LECs.[35]

The basic requirement for electroluminescence in organic semiconductors (such as a luminescent polymer) is that electronic charges (holes and electrons) can be injected and meet. In organic materials holes can be injected into the highest occupied molecular orbital (HOMO), and electrons into the lowest unoccupied molecular orbital (LUMO), given that the work functions of the anode and cathode, respectively, are well matched to these energy levels.[17] The energy difference between the HOMO and the LUMO corresponds to the energy

[iv] In fact the angular "sweep" is one dimensional and for the polar angle only; we assume azimuthal symmetry. An integrating sphere collects the light emitted in all directions, which is good for some purposes. However, it is obvious that no angular dependence can be attained from such measurements.

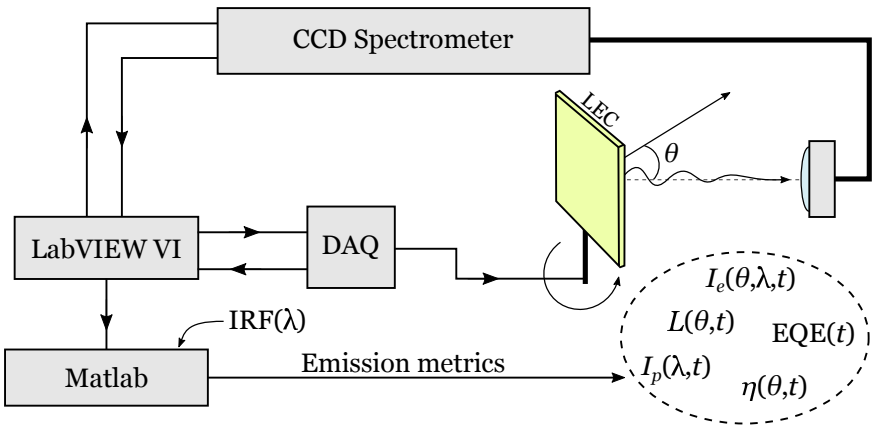

Figure 2.5: Schematic of the custom-built spectroscopic goniophotometer set-up. A LabVIEW virtual instrument controls and synchronizes the rotation of the sample and the collection of the raw emission spectra. The collected data is post processed in Matlab to give a number of luminous and radiant emission metrics resolved or integrated with respect to viewing angle and/or wavelength.

gap (E_g) of the material. A hole and an electron have opposite electric charge, and are therefore electrostatically attracted to each other. As they meet in an organic semiconductor they form an "exciton", a quasiparticle that corresponds to an electrostatically bound electron-hole pair.[48] An exciton eventually decays, which figuratively means that the electron jumps into the hole and its excess energy dissipates radiatively as light with a wavelength given by Eq. (2.1), or non-radiatively eventually turning into heat.

Organic semiconductors such as conjugated polymers are soft in comparison to their inorganic crystalline equivalents. An introduced additional electronic charge carrier, be it an electron or a hole, is therefore comparatively localized and interacts strongly with the surrounding material. Together, the electronic charge and the surrounding material it interacts with, can be described by another quasiparticle called a "polaron". The name reflects the local polarization and the chemical-conformation changes of the polymer that it brings.[45]

If mobile ions are present in the luminescent polymer layer, thus forming the active layer of an LEC, the requirement of matched electrode work functions for efficient charge injection is relaxed. In fact, an anode and cathode made out of the same material can be used. This is commonly not the preferred structure in a practical sandwich device. At least one of the electrodes needs to be semi-transparent in order for the generated light to escape the structure, and by using a reflective second electrode the backwards emitted light can be redirected into the forward hemisphere. Nevertheless, equal electrodes make for a good explanation case, and are used in the schematics in Fig. 2.6.[31] The ion action during

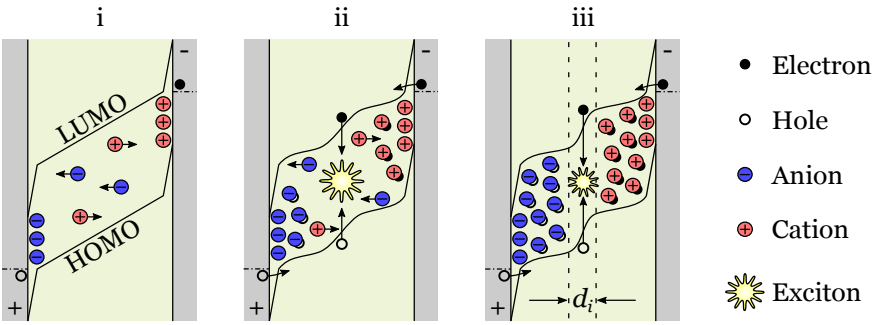

Figure 2.6: The redistribution of ions and shift of energy levels during the turn-on process of an LEC. i) Just after a bias is applied to the electrodes, ionic electric double layers form at the electrode interfaces and screen the electric field in the bulk from the electrodes. ii) When electronic charges are injected into the HOMO and LUMO of the luminescent polymer they are electrically neutralized by ions, which prevents the build-up of space charge. Ideally, most of the injected holes and electrons at this stage form excitons that generate light. iii) When all accessible ions are locked up in electrochemical doping units or electric double layers, an intrinsic region depleted of ions (of width d_i) is left in between the p- and n-type doped charge-transport regions. Excitons form, but the emission is partly quenched by the doping.

the transient LEC operation at constant voltage can somewhat simplified be described by the following three stages:

i. As the device is first biased, the original ion distribution in the emissive layer changes and the dissolved and mobile ions drift in response to the imposed electric field between the electrodes; negative anions move towards the anode, and positive cations towards the cathode. At each electrode interface they accumulate and form an (ionic) electric double layer. This uncompensated layer of space charge screens the electrostatic potential in the luminescent polymer so that the potential barrier at the interface shrinks, which facilitates injection of a hole (or electron) into the HOMO (or LUMO), see Fig. 2.6. At this stage the electronic current density through the device is very low or zero, but it increases quickly, as shown in region "i" in Fig. 2.7a.

ii. When holes (or electrons) get injected into the HOMO (or LUMO) they chemically oxidize (or reduce) the luminescent polymer, and some of them will be electrically compensated by a continued ionic redistribution.[v] The complex consisting of an oxidized (or reduced) luminescent polymer site

[v] The polarons that are not compensated by ions will (if charge balance allows) form excitons and decay as light or heat. Else they might simply traverse the active layer and be collected at the other electrode, although the latter becomes highly improbable when a doping structure has formed.

and a compensating ion, is termed an electrochemical doping unit. p-type (hole) doping taking place at the anode, and n-type (electron) doping at the cathode, as shown in Fig. 2.6. In highly doped organic semiconductors, the increased density of electronic charge carriers, or polarons, results in a strongly enhanced conductivity.[17] The conductivity increases with the number of electronic charge carriers according to Eq. (2.4), where γ is the conductivity, n is the number density of electrons, p is the number density of holes, e is the elementary charge, and $\mu_{n,p}$ is the mobility of the electrons (or holes). Note, that in electrochemical doping, the additional electronic charge carriers are supplied through electrochemical reactions (injection from the electrodes), rather than by the replacement of atoms with a different atomic number as is done for chemical doping of inorganic semiconductors. The current density through the device is now substantial, and it increases as the doping process continues, see region "ii" in Fig. 2.7a.

$$\gamma = e(n\mu_n + p\mu_p) \tag{2.4}$$

iii. As more electrons and holes are injected into the luminescent polymer, the number of electrochemical doping units in the active layer increases. Consequently, the electrochemically doped transport regions grow towards each other, and/or the doping concentration (σ) within them increases. The competition between these two processes during the turn-on phase of sandwich LECs is unclear, and has as far as I know not yet been studied. When the device has become "fully" doped it is void of free ions, and a non-doped and ion free "intrinsic" region of width d_i is left between the p- and n-type doped *transport* regions, as shown in Fig. 2.6. During the doping process the width of the non-doped region decreases, and the conductivity of the transport regions increases. Together these two effects result in a lowered overall device resistance that is manifested by the increasing current density in regions "i" and "ii" in Fig. 2.7a, which levels out as the device becomes fully doped in region "iii".

The intensity of the light emission from an LEC varies during the turn-on process, which is inherently connected to the electric processes described above. Typically, the luminance initially follows the increasing driving current density, but reaches a maximum and starts decreasing before the current density levels out, compare Fig. 2.7a and b. The luminous current efficacy evolution has a sharp initial increase that stems from the more balanced injection of electrons and holes that follows the formation of electric double layers and electrochemically doped transport regions. The current efficacy also has a maximum, but it occurs before that of the luminance, as shown in Fig. 2.7c. The decreasing luminance and current efficacy can be explained by a process called "exciton-polaron quenching". Briefly put this means that the radiative decay pathways

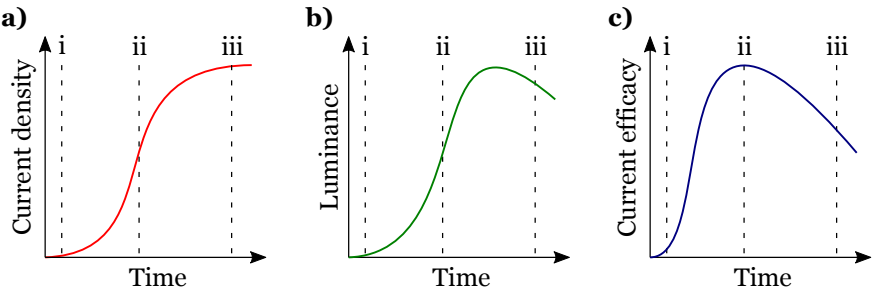

Figure 2.7: A qualitative description of the evolution of device properties during the three turn-on stages at constant voltage driving. **a)** The current density, **b)** the forward luminance, and **c)** the current efficiency.

(light emission) for an exciton are less likely than other (non-radiative) pathways when the exciton is close to a polaron (i.e. doping).[49] I will return to this subject in chapter 6. It should be mentioned that the exact shape and position of the luminance- and efficacy curves and maxima can vary between different material combinations, and that the expected drops explained here to some extent can be alleviated by controlling the amount of ions during fabrication of the devices. A lower available ion concentration will give a wider intrinsic region and reduced exciton quenching by polarons, but at the same time the current density (and therefore the luminance) at a given voltage will be lower because of the higher resistance of the device.[50, 51]

The electric operation of LECs described above, with its *in-situ* evolution of an electrochemically doped device structure, suggests that the *optical* structure could change correspondingly. But application wise, electrochemical doping also allows for some quite interesting architectures of light-emitting devices. For example, planar LECs with a µm–mm thick active layer, and electrodes positioned side by side, give direct visual access to the active layer. Thus, the size allows for it to be probed *in-operando* in order to learn about the internal structure evolution of LECs.[52, 53] Another architecture is the bilayer LEC, in which the electrolyte and luminescent polymers are intentionally separated, which allows for some interesting properties and possibilities.[54]

3. Line art and pixels: The bilayer architecture

THE STRUCTURE OF A BILAYER LEC is different from that of an ordinary LEC in the sense that the active layer is split into two stacked layers: one electrolyte layer, and one layer with the luminescent polymer.[55] For bilayer LECs in a sandwich configuration, i.e. where the active layer(s) together with the electrodes make a stratified stack, electronic contact between the electrodes requires that the electrolyte layer is patterned in the lateral plane.

3.1 Fabrication of the bilayer

In paper **II** we use a direct-write sequential spin coating method where we first spin coat the electrolyte phase (KCF_3SO_3 and high molecular weight PEO) from a cyclohexanone-based electrolyte ink onto the ITO anode. We then remove parts of the solid electrolyte film with a sharp stylus to create a line-art pattern. On top of the patterned electrolyte film we spin coat Super Yellow from a toluene-based ink to form an emissive layer. After drying the bilayer stack, a thin aluminium cathode is deposited by physical vapour deposition.

In paper **I**, the interruption of the electrolyte phase is instead of manual scratches in a homogeneous solid film, achieved during its deposition. We use a material inkjet printer to deposit well-defined and separated droplets of electrolyte (KCF_3SO_3 and low molecular weight PEO) in a computer controlled pattern. Because of the minute size of the ejected droplets (10 pl), they dry very quickly after landing on the ITO-anode surface. The emissive Super-Yellow layer is then deposited by spin coating, and the aluminium cathode by physical vapour deposition, just as for the line-art devices.[vi]

[vi] To preserve the bilayer structure during deposition of the luminescent polymer, it is important to find a solvent that does *not* dissolve the underlying solid electrolyte. For this reason we used toluene, which is a good solvent for Super Yellow, but very poor for PEO and KCF_3SO_3. In hindsight it would probably have been better to use e.g., anisole for depositing the emissive layer, as it has less adverse effects on health and environment, and should fulfil our solubility requirements.[56]

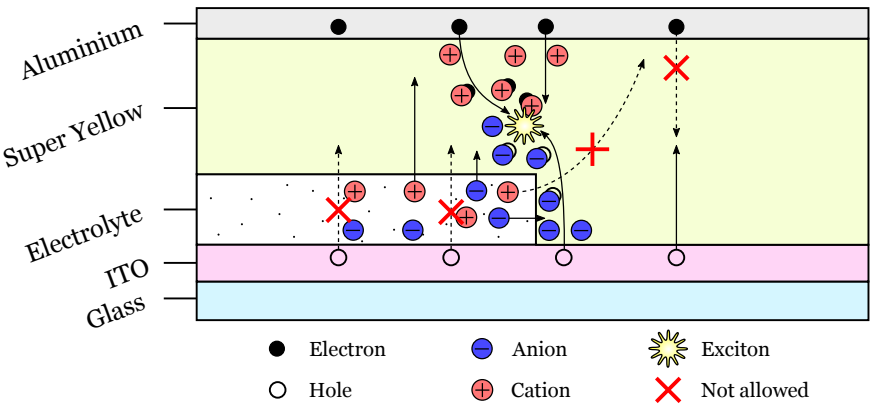

Figure 3.1: Cross section of a bilayer LEC in sandwich configuration and its operation mechanism. Cations from the electrolyte phase must enter and drift across the emissive layer to reach the cathode and allow for electron injection through double layer formation and doping. Holes can be injected from the electrolyte free regions. Excitons and light form in the regions with overlapping electron and hole injection.

3.2 Bilayer electric operation

Given the electric operation mechanism of a common sandwich LEC with a mixed active layer (see section 2.4), a thought experiment can visualize how a bilayer LEC should work. First of all, most non-conjugated polymers (such as PEO) are *electronic* insulators although they can be good *ionic* conductors. The part of the ITO anode that is covered by the PEO-dominated electrolyte phase is therefore electronically passivated or masked, with no hole injection. Second, the energy levels of ITO, Super Yellow, and aluminium imply that no light can be expected without electric double layer formation and electrochemical doping. The reason is that the work function of aluminium is too high for efficient injection of electrons into the LUMO of Super Yellow. Holes on the other hand, can to some extent be injected from the ITO into the HOMO of Super Yellow, but it takes two to tango: no excitons will form unless *both* electrons and holes are injected. Third, the ions are located in the separated electrolyte phase instead of being intimately mixed within the emissive layer, so they have to enter and travel in the non-polar emissive Super-Yellow layer in order for balanced injection of electrons and holes to occur, see Fig. 3.1. Thus, the lateral distance that cations are transported in pure Super Yellow determines the extent of the emissive regions away from the electrolyte phase, e.g. into the regions between inkjet-printed electrolyte droplets.[vii] Likewise, the lateral extension of

[vii] Here, "pure" does not refer to the purity of the polymer, but rather to the exclusion of ion-transporting material and salt.

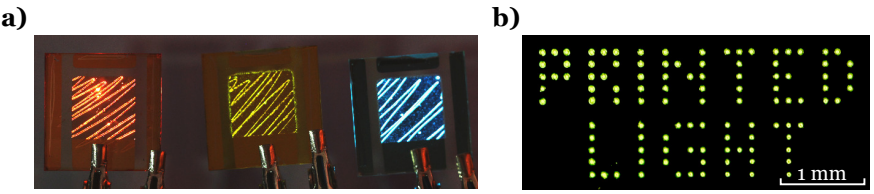

Figure 3.2: Steady-state light emission from patterned bilayer LECs. **a)** Subtractively patterned line-art devices with three different luminescent polymers (to scale). **b)** An inkjet-printed pixelated device displaying two indicative emissive words.

the p-doped regions that conducts holes, determines the extent of the emissive regions above (or "into") the electrolyte, e.g. towards the centre of the electrolyte droplets, or away from the scratch regions. At this point it is important to remember that as the device is biased, a large electric field (in the order of $MV\,m^{-1}$) drives the electrically charged ions in the direction from one electrode to the other, whereas lateral ion transport is primarily driven by diffusion.

3.3 Patterned emission

The light emission at steady state from three line-art bilayer LECs are shown in Fig. 3.2a.[viii] It seems to follow the operation mechanism outlined above, as only the scratches in the electrolyte phase are emissive. Of course, the manually drawn back-and-forth pattern could easily have been replaced by a light-emitting signature or similar. The light emission from a "pixelated" bilayer LEC, fabricated using the additive inkjet technique, is shown in Fig. 3.2b. The separated droplets are positioned by the printer to form pixels and the words "PRINTED LIGHT". At this scale it appears as if the full droplet regions are emissive, with no emission from the non-patterned regions.

These results are exciting from an application point of view, as they showcase that customizable light-emitting patterns can be achieved in both a manual and an automated and programmable way without the need for complicated electrode patterning. But let us not jump to conclusions just yet. The electrolyte-covered regions in the line-art devices in Fig. 3.2 are as expected (with no hole injection) not emissive. However, according to the same argument the electrolyte *covered* droplets in the inkjet-printed devices should be non-emissive and the region between the droplets should emit light. This contradicts our observations: the droplets are emissive pixels and the region around them is dark and non-emissive. To see what the emission looks like in more

[viii] Two other luminescent polymers where also tested as the emissive layer in paper **II**: one with red and one with blue emission.

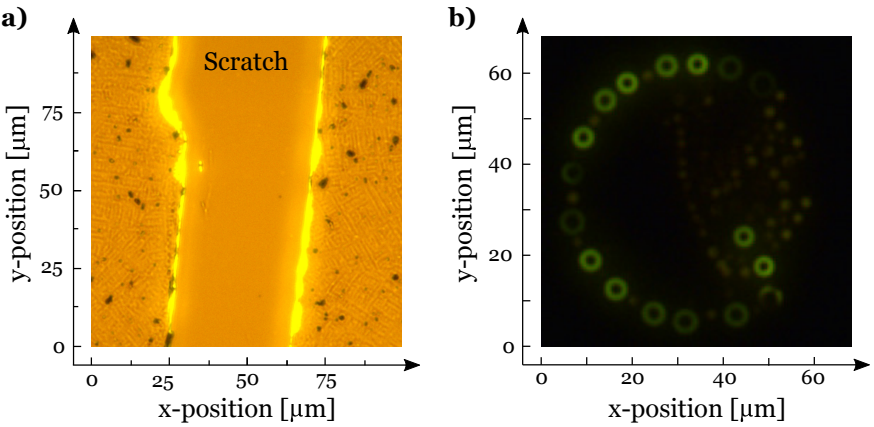

Figure 3.3: Micrographs of emissive features in bilayer LECs. **a)** The scratch region in a line-art device. **b)** A single droplet region in a pixelated device.

detail, and check how our operation hypothesis holds or fails, we decided to investigate the emissive regions further using optical microscopy.

Micrographs of line-art and pixelated bilayer LECs are shown in Fig. 3.3a and b. Clearly, the emission of the line-art device, that by the naked eye was perceived as one line, is in fact two separated lines located above the interlines between electrolyte, Super Yellow, and ITO, and with a non-emissive central part. Likewise, what seemed like homogeneous pixel emission is under the microscope broken into smaller circles, each corresponding to the same interline as for the line-art device. As seen from the height profile of a dry electrolyte droplet in Fig. 3.4, the inkjet-printed wet electrolyte droplet has dried in a broken coffee-ring like fashion, with multiple pinning lines and exposed ITO within the droplet perimeter.[57] These microscopic observations are reassuring, and support that our hypothesized model of operation is applicable to both kinds of devices. The light emission *is* limited to the regions around the interlines, and the lateral extension of the light emission into regions above electrolyte-free regions (such as the scratch in the line-art devices or between the electrolyte droplets in the pixelated devices) is smaller than the resolution of micrographs. To some extent, however, the emissive regions grow with time towards the electrolyte covered regions (< 5 µm in the investigated material systems), which can be explained by an imperfect electrolyte film at the edges, or that the high conductivity of the p-type doped Super Yellow effectively works as an extension of the anode, and reaches in over the insulating electrolyte phase.

We can summarize the operation model for the bilayer LEC as follows: Cations can drift (and diffuse) across a thin layer (on the order of $100 - 200$ nm) of pure Super Yellow that is void of ion transporting material, but do not appear

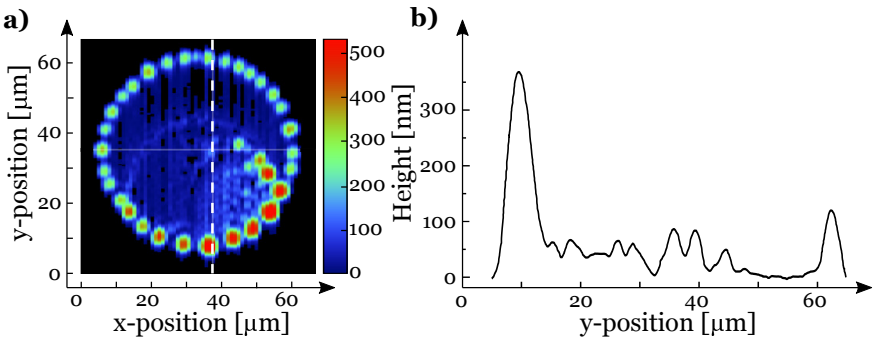

Figure 3.4: Height profile of a dry inkjet-printed electrolyte droplet. **a)** A 2-dimensional map. **b)** A cross section along the vertical white dashed line in a.

to diffuse larger distances (on the order of micrometres) laterally from the electrolyte covered regions. Holes are injected from electrolyte-free regions, and they overlap spatially with injected electrons only above the interlines of electrolyte, Super Yellow, and ITO. Accordingly, it is only in this limited region that light is generated.

3.4 Effects of high doping concentration

In LECs with a mixed active layer it is well established that the initial salt concentration is important for several key characteristics, including the turn-on time, luminance, and the efficiency, as described in section 2.4.[41, 58, 59] In papers **I** and **II** we have proved the concept of patterned light-emission from bilayer LECs and established a model for their operation, but we did not try to optimize the salt concentration. In fact, this would likely turn out to be difficult, given that the total number of ions changes with the electrolyte volume in the device. In addition, we lack a proper estimate of the fraction of the available ions that can take part in electrochemical doping: some ions are probably locked up in semi-crystalline PEO, and some may be too far away from the emissive regions to contribute.

It would probably be much easier to get efficient patterned LECs by using a standard mixed active layer, and replace the PEO-electrolyte film with another electronically insulating polymer. For example, a UV-curable photoresist film (such as SU-8) would enable photolithographic methods and high-resolution patterns, although this would complicate the fabrication process and reduce the manual adjustability. The quality of the emission from the LECs would benefit from a reduction of the sprinkled background emission seen in the blue device in Fig. 3.2a (it originates in poor quality and high number of pinholes in the

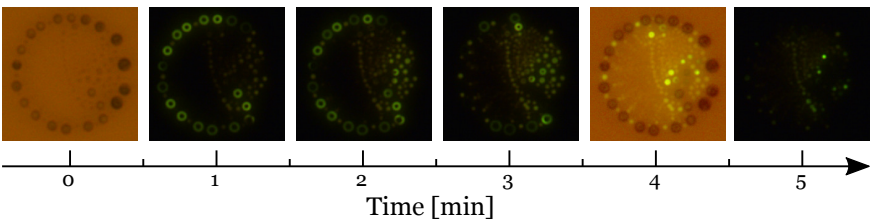

Figure 3.5: Time-lapse micrographs of a pixel region during operation of an inkjet-printed device. The starting image (at t = 0 min) of a doped device is captured under illumination of the microscope lamp, just like the image at t = 4 min. The time difference between each of the images is approximately one minute.

PEO-electrolyte film). We could also expect an enhanced efficiency because of the improved spatial overlap between hole and electron injection.

It is well established that the absorption of conjugated polymers changes during doping, and this effect is called electrochromism.[60] For a biased pixelated device this enhanced absorption shows in the form of dark regions under illumination, see the starting image in Fig. 3.5.[ix] The darkening corresponds precisely to the electrolyte-droplet height profile in Fig. 3.4, which is distinct evidence that the bilayer devices are doped only in the vicinity of the electrolyte regions, and that Super Yellow is electrochromic. Interestingly, from a time-lapse comparison of the electroluminescence of a pixel region in Fig. 3.5, we can also see that the extension of the microscopic emissive region changes drastically: The inner part of the droplet—with little electrolyte but a lot of pinholes—initially becomes brighter with time, whereas emission around the perimeter fades. After a few minutes the doping concentration seems to have reached a high enough level to almost completely quench the electroluminescence. Similar trends could be seen in the line-art devices, where the initial growth of the line width was reversed as the quenching set in at high doping concentrations (these data were actually not shown in paper **II**).

Efficient light generation in bilayer LECs is enabled by electrochemical doping of the active layer, but interestingly we here see how it can also become a limiting factor at high doping concentration. The doping-induced absorption and electroluminescence-quenching observations point to important questions for the whole LEC field: How will the luminous properties and efficiency of sandwich devices be affected by the doping-dependent optical properties of the luminescent polymer? And what can be said about their optical operation as a result of this?

[ix] Because of the small overlap between the lamp spectrum (blackbody emission at 3100 K) and the absorption of non-doped Super Yellow, the darkening is likely caused by an altered absorption rather than being an effect of photoluminescence quenching.

4. Optical response to doping of a luminescent polymer

WITH THE VISIBLE CHANGES TO ELECTROCHEMICALLY DOPED SUPER YELLOW in the bilayer LECs of chapter 3, it is clearly of interest to quantify how the optical properties change with electrochemical doping concentration. The complex refractive index, $n' = n + i\kappa$, where n is the refractive index and κ is the extinction coefficient (i is the unit imaginary number), is a complete measure of the optical properties. κ is related to the absorption coefficient α according to Eq. (4.1). Depending on the setting it can be cumbersome to measure n' appropriately. Translucent materials (e.g., Super Yellow), with absorption in or close to the visible wavelength range, will have a refractive index and extinction coefficient that vary strongly with wavelength, so the measurement must be spectral and cover the full visible range. In addition, we are after the complex refractive index of a solid film of Super Yellow, and not in solution.

$$\alpha = \frac{4\pi\kappa(\lambda)}{\lambda} \tag{4.1}$$

The go-to choice for complex refractive index measurements of thin films is ellipsometry. In ellipsometry, polarized monochromatic light illuminates a thin film of the investigated material, and the change of polarization upon reflection is detected and related to the refractive index. Spectral ellipsometry uses a polarized broad-band light source, and can therefore give the spectral complex refractive-index values of the sample following some oscillator modelling.[61] It is a commercially available and powerful technology, but not ideally suited for our purpose: we also require the measurements to be performed at precisely controlled doping concentrations. This complicates the measurements substantially, as it requires an integrated electrochemical set-up that is synchronized to the collection of the ellipsometry data.

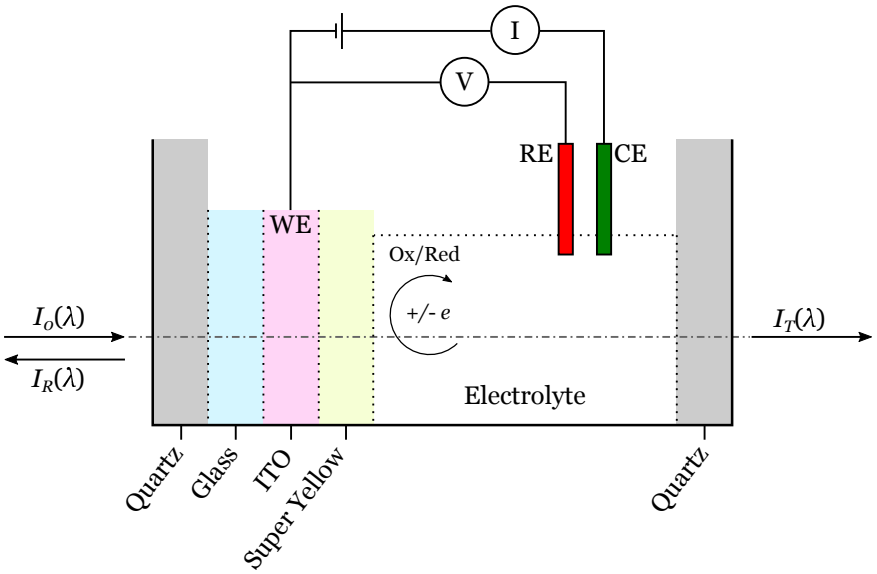

Figure 4.1: Schematic description of the spectroelectrochemistry set-up. The optical path through the quartz cuvette, sample, and liquid electrolyte is shown, as well as the wiring to the working electrode (WE), reference electrode (RE), and counter electrode (CE) of the cyclic voltammetry set-up. The collection optics and spectrometers are not shown.

4.1 The spectroelectrochemistry method

Instead of using ellipsometry, we in paper **III** opted to use a simpler and more modular method—spectroelectrochemistry. This is a common method for investigating the change in absorption spectrum during electrochemical doping.[x] To get a full optical characterization we simultaneously measured both the reflection $\left(I_R(\lambda)\right)$ and transmission intensity spectra $\left(I_T(\lambda)\right)$ as the sample underwent electrochemical doping. These measurements were then coupled with thin-film optics simulations and oscillator modelling to get the doping-dependent complex refractive-index spectra. The method is schematically depicted in Fig. 4.1 and can briefly be described by the following three main components:

i. A cyclic-voltammetry set-up used to electrochemically p-dope *or* n-dope a thin film of Super Yellow on an ITO working electrode.

[x] It is very common to do only transmission measurements and assume that the absorption is $1 - I_T/I_0$. However, also the reflected intensity spectrum might depend on the optical properties of the sample, which could make the former a poor approximation, at least for thin solid films.

ii. A spectroscopy set-up with an illumination source and two spectrometers that simultaneously collect $I_R(\lambda)$ and $I_T(\lambda)$ of the electrochemical system stack. The collection is automatically repeated with a short time interval to capture the evolution of the spectra as the Super-Yellow film undergoes electrochemical doping.

iii. A thin-film optical analysis built on the transfer-matrix formalism, and a routine to extract the complex refractive index of the Super-Yellow film at different times and doping concentrations from the experimental reflectance and transmittance spectra.

In cyclic voltammetry the electric potential is scanned, and the electroactive compound (in our case Super Yellow) is electrochemically p- or n-type doped depending on the direction of the scan. When the potential scan is reversed, some of the doping relaxes, which is seen by a sign change of the current trace. A typical cyclic voltammogram of Super Yellow is presented in Fig. 4.2a, where also the onset potentials for p- and n-type doping are marked by dashed vertical lines.

The doping concentration (σ) during the experiment is given in unit of dopants per polymer repeat unit (r.u.$^{-1}$), as described in Eq. (4.2). The total amount of injected charge (Q) is gained by integrating the current between the ITO working electrode and the silver counter electrode with respect to time, N_A is Avogadro's number, ρ is the mass density and $\widetilde{V}$ the volume of the undoped polymer film, e is the elementary charge, and M_{w}^{SY} is the molecular weight of the average Super-Yellow polymer repeat unit.

$$\sigma_{p/n} = \frac{Q_{p/n} M_{\mathrm{w}}^{SY}}{\rho N_A \widetilde{V} e} \tag{4.2}$$

The spectroscopy was performed in a collimated fashion where we took great care during alignment to ensure normal incidence of the illumination beam onto the cuvette, and to collect the entire transmitted beam with the collection lens of the transmittance spectrometer. Thus, energy conservation for the light beam can be expressed as $1 = R(\lambda) + T(\lambda) + A(\lambda)$, with R, T, and A being the reflectance, transmittance, and absorptance of the experimental stack, respectively.

By plotting $1 - R(\lambda)$ and $T(\lambda)$ in the same graph, the separation between the curves corresponds to the absorptance of the experimental stack. The absorptance for a pristine (non-doped) thin film of Super Yellow in an empty cuvette (with no electrolyte) is shown this way in Fig. 4.2b.

The simulated reflectance and transmittance spectra for a stack depend on the complex refractive index of the included materials. Thus, we can now extract the complex refractive index of pristine Super Yellow through a

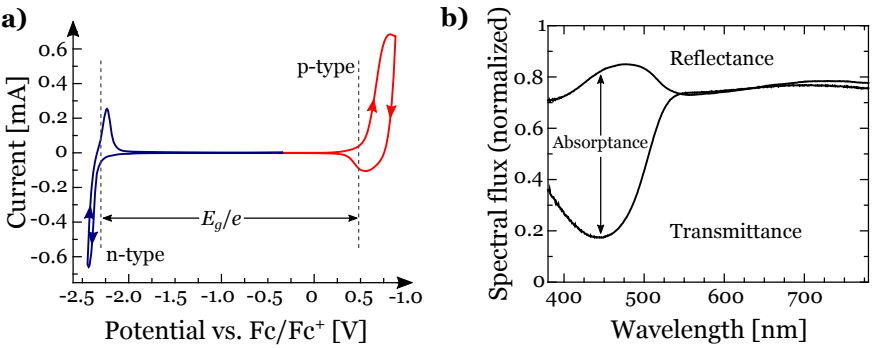

Figure 4.2: a) A cyclic voltammogram of Super Yellow. **b)** The reflectance and transmittance spectra of a thin film of Super Yellow in the measurement set-up without the electrolyte and in the pristine non-doped state.

least-squares minimization of the difference between the simulated and experimental reflectance and transmittance spectra, Δ_{TR}, according to Eq. (4.3). The extracted n and κ spectra are presented as the black solid lines in Fig. 4.3, and we find that the extinction coefficient is strong with a maximum of 0.58 at $\lambda = 450$ nm but essentially zero at $\lambda > 550$ nm. The refractive index has a peak of 2.10 at $\lambda = 485$ nm, and decreases monotonically to 1.75 at $\lambda = 800$ nm. Both n and κ are in good agreement with literature and ellipsometry data on non-doped Super Yellow.[62] Importantly, during the extraction the complex refractive index of Super Yellow was modelled with a Kramers-Kronig consistent Tauc-Lorentz oscillator, which ensured a physically sound relation between the real and imaginary part.[45]

$$\Delta_{TR} = \sum_{\lambda} \left(R_{exp} - R_{sim}\left(n_{\sigma}^{lSY}\right) \right)^2 + \sum_{\lambda} \left(T_{exp} - T_{sim}\left(n_{\sigma}^{lSY}\right) \right)^2 \tag{4.3}$$

4.2 Doping-dependent refractive-index spectra

With electrochemical doping comes a polaron-absorption band in the near-infrared region, which is responsible for the dark regions in Fig. 3.5.[63] By adding a second Tauc-Lorentz oscillator to the model, to account for this absorption band, we can get good fits of the simulated and experimental reflectance and transmittance also for electrochemically doped Super Yellow films.

The resulting doping-dependent refractive-index spectra are presented in Fig. 4.3a and c, and the corresponding extinction coefficients in Fig. 4.3b and d. For both p- and n-type doping we find a lowering of the refractive index and extinction coefficient in the short wavelength range, which can be described

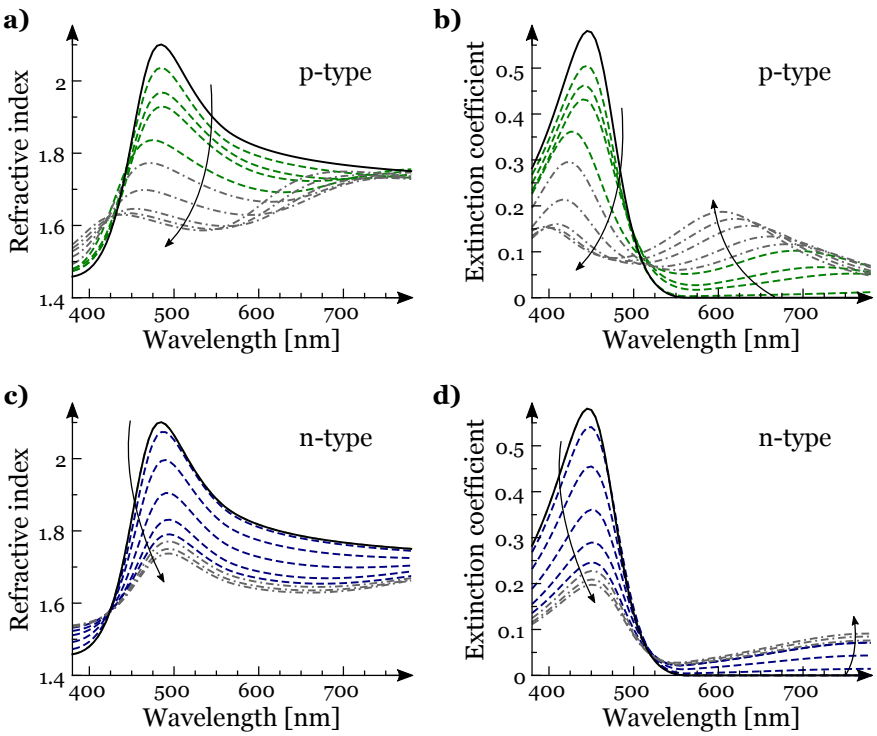

Figure 4.3: Refractive-index and extinction-coefficient spectra of electrochemically doped Super Yellow at different doping concentrations. **a)** and **b)** The effects following an increasing p-type doping concentration from $0-0.2$ r.u.$^{-1}$ (green dashed lines). **c)** and **d)** The effects of increasing n-type doping concentration from $0-0.6$ r.u.$^{-1}$ (blue dashed lines). Grey dash-dotted lines show extrapolations from the measurements to 1 r.u.$^{-1}$.

as a bleaching of the $\pi - \pi^\star$ transition that corresponds to exciting an electron from the HOMO to the LUMO.[60] Simultaneously, a polaron-absorption band emerges in the red to near-infrared part of the spectrum.[64] The response to doping is for both p-and n-type doping highly non-linear, with the biggest effects occurring at the onset of doping whereafter the rate of change decreases. Surprisingly, there are also notable qualitative differences between the complex refractive indices of p- and n-type doped Super Yellow. For example, the doping-induced features for p-type doping are blue shifted with increased doping concentration, whereas they are red shifted for n-type doping. Also the magnitudes of the shifts are different. p-type doping is more "potent" than n-type doping, and reaches similar values of both refractive index and extinction coefficient at one third of the doping concentration (0.2 compared to 0.6 r.u.$^{-1}$). For experimental integrity reasons, we performed the potential scan at a high rate of 50 mV s^{-1}, and we opted to limit the amount of doping to 0.2 and 0.6 r.u.$^{-1}$ for p- and n-type doping, respectively. As we will see in chapter 5, doping concentrations close to 1 r.u.$^{-1}$ are required for simulations of LECs, and for this reason we have *carefully* extrapolated the derived values, and present these results as grey lines in Fig. 4.3.[xi]

To pinpoint the cause for the asymmetric response between p- and n-type doping of Super Yellow, and analyse the electronic transitions in more detail, further investigations using e.g., x-ray or ultraviolet photoemission spectroscopy are probably required.[65] Theoretical studies on the closely related polymer poly(*para*-phenylenevinylene) report that there should be virtually no difference between p-and n-type doping in general.[66] However, several experimental observations indicate that this might not be the case, and our results add to that picture.[53, 63, 67] It would be interesting to see whether the asymmetry is a general feature for luminescent conjugated polymers, or if it for some reason is specific to Super Yellow. However, the time for research and the scope of a thesis are both limited. Instead of scrutinizing the cause of the asymmetric n and κ spectra of doped Super Yellow, we acknowledge and note their differences, and keep them in mind as we continue on the path towards an optical operation model for LECs.

[xi] With the experimental results at hand we could probably safely have extended the measured doping range, for both p- and n-type doping, and used a lower potential scan rate. Our main concern at the time was dissolution of the doped polymer film in the liquid electrolyte, but measurements showed that the film thickness increased with doping, which indicates that the film had not been dissolved.

5. The consequences of being thick: Experiments and modelling

THE ACTIVE-LAYER THICKNESS (d_{al}) of an LEC can easily be adjusted in the fabrication process (e.g., by adjusting the rotational speed during spincoating). d_{al} is usually about 100 nm for lab-scale research. But in upscaled solution-based production a thickness on the order of a few hundred nanometres might be required to get active-layer films that are free from short-circuiting pinholes. Despite being an important step in taking LECs from research to applications, how such a d_{al} increase affects the luminous output of the devices has to a large extent been overlooked in the scientific discussion.[68, 69] In paper **IV** we investigate the experimental effects of d_{al} in a Super-Yellow based sandwich LEC. The thickness of the active layer is also a suitable variable when comparing experiments and simulation results from an optical model, which we do in paper **V**. As it turns out, LEC optics is an intriguing and non-trivial subject with significant effects on the luminous output of devices following changes to, for example, the active-layer thickness.

5.1 Operating voltage and forward luminance

Six LECs, with an active layer consisting of Super Yellow, TMPE-OC and $LiCF_3SO_3$ in a mass ratio of 1:0.2:0.03, and with thicknesses of 100, 130, 180, 230, 300, and 380 nm, where fabricated according to the description in chapter 2. The devices where driven at a constant current density of 25 mA cm^{-2} and characterized using the spectroscopic goniophotometer described in section 2.3.3. All six LECs feature the typical operating voltage evolution introduced in chapter 2, with a decreasing operating voltage following electrochemical doping of the active layer, see Fig. 5.1a. The voltage curves level out after approximately 180 minutes, which we define as the steady state for the now fully doped LECs. The steady-state voltage increases with the active-layer thickness—which is not surprising since it simply means that the overall resistance increases with

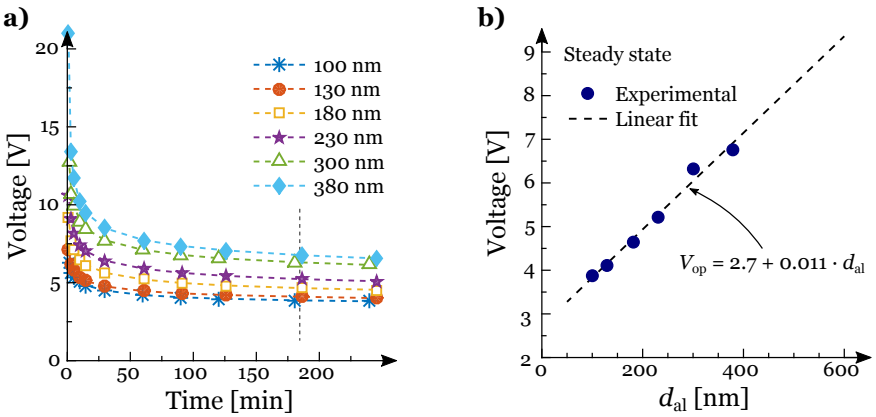

Figure 5.1: Operating voltage characteristics. **a)** Evolution of the operating voltage of LECs with different active-layer thickness. **b)** Steady-state operating voltage versus the active-layer thickness.

thickness—and the relation is essentially linear, as shown by the linear fit in Fig. 5.1b.

Electrically, the devices with different thickness all follow our expectations and they can thus be seen as well behaved. But when it comes to the forward luminance, the picture is quite different: The luminance evolution curves are qualitatively distinct, with the 100, 130, and 300 nm devices exhibiting the normal turn-on behaviour with an increasing luminance (see section 2.4), whereas the luminance of the 180 and 230 nm devices actually decreases with time. Instead of a monotonic trend, the steady-state luminance in Fig. 5.2b displays periodic character with respect to d_{al}, with two local maxima at 100 and 300 nm, and a distinct minimum in between.

In addition to these somewhat unexpected forward-luminance results, we find that the emission colour of the devices varies more than we had expected, as displayed by the photographs in Fig. 5.3. The characteristic yellow emission of Super Yellow for the 100 nm device shifts with increasing thickness to orange, green, yellow, and orange again for the 380 nm thick device. During characterization, we could also observe significant colour changes with both viewing angle and time for the thicker devices between 180 and 380 nm.

5.2 Setting up an optical model

It is trivial that an absorbing material attenuates the intensity of light that passes through it. The transmitted light intensity decreases exponentially with the

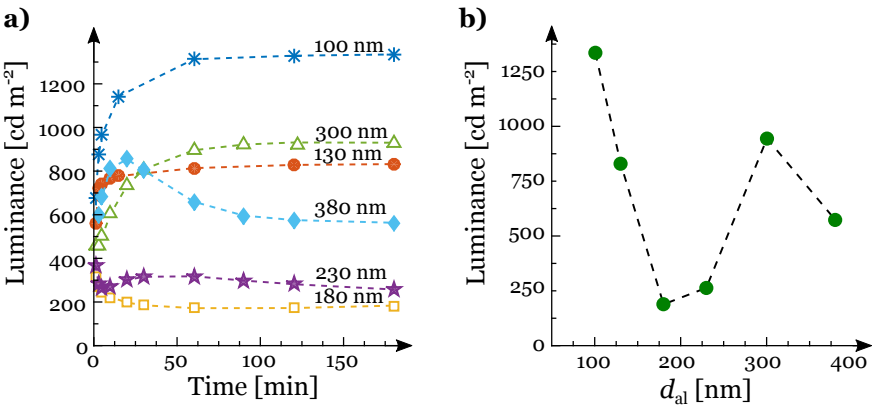

Figure 5.2: Operating luminance characteristics. **a)** Evolution of the forward luminance of LECs with different active-layer. **b)** Steady-state forward luminance versus the active-layer thickness.

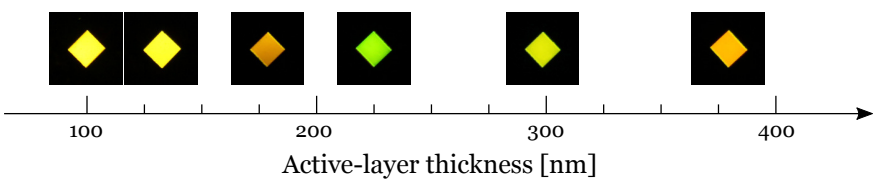

Figure 5.3: Photographs displaying the emission colour in the forward direction at steady state as a function of active-layer thickness.

thickness of the absorbing layer, following the so called Beer-Lambert's absorption law. The extinction-coefficient spectrum of electrochemically p- and n-type doped Super Yellow in Fig. 4.3 overlaps with the photoluminescence spectrum in Fig. 2.4c. Therefore, absorption in the doped transport regions must be taken into consideration in an optical model of our LECs.[63] However, we observe a number of trends which deviate from what can be expected from the absorption alone: The thickness dependence of the forward luminance is periodic rather than showing a monotonic decrease, as seen in Fig. 5.2b. The emission colour in Fig. 5.3 varies with thickness in a periodic way, instead of being blue shifted (which would be expected from the spectral overlap between absorption and emission). In paper **IV** we found that the angular emission intensity was periodic with thickness. At this stage it is useful to acknowledge that our LECs are thin-film multilayer structures with a reflective aluminium electrode and an ITO-covered glass substrate surrounding the electrochemically doped active layer. The refractive-index differences between these layers gives that non-negligible internal reflections can be expected. Interference effects are

plausible because the optical thickness of the active layer and the semitransparent ITO anode is comparable to the wavelength of the emission.[45, 70]

Software for efficient coherent simulations of multilayer optical devices is already commercially available, with one example being setfos 4.6 developed by Fluxim AG. This software uses the transfer-matrix formalism to compute the propagation of light in a stratified stack, which requires that the thickness and complex refractive index of each constituent layer of the simulated structure is known. The complex refractive index of the glass substrate and the aluminium cathode are given in the scientific literature, and we have measured it for ITO and Super Yellow in both its pristine state and for different p- and n-type doping concentrations as disclosed in chapter 4.[44, 71, 72] But LECs have doped transport layers with a spatial doping-concentration profile, and since this doping profile is unknown during the dynamic turn-on of the device, so is the "optical profile" (the spatial profile of the refractive-index and extinction-coefficient spectra across the device). To facilitate the analysis, we decided to limit the scope from the time-dependent case to the steady state. We can then assume that all ions take part in electrochemical doping, which for our investigated devices (with a molar Super Yellow:$LiCF_3SO_3$ ratio of 1:0.065) corresponds to an average doping concentration of 0.13 r.u.$^{-1}$. On the basis of charge conservation and redox balance, the number of p- and n-type dopants in the device must be equal (given that there are no electrochemical side reactions).[59, 73] But to get a complete optical profile of the active layer, we must also answer the following three challenging questions:[xii]

i. What is a realistic shape of the doping profile in the transport regions at steady state?

ii. How wide is the intrinsic region, and (how) does it change with the thickness of the active layer?

iii. Where in the active layer is the intrinsic region located?

5.2.1 Parametrization of the optical profile

First, van Reenen et al. have showed that a constant gradient is a reasonable assumption of the doping-concentration profile in the active layer at steady state, i.e. a linearly decreasing doping concentration from the electrodes to the edges of the intrinsic region. They argue that at steady state there is no net ion current, which in a biased LEC occurs only if the ionic drift- and diffusion-current components cancel. This steady state corresponds to the case when the device

[xii] Because of the very thin active layer in sandwich LECs, none of these questions have yet been answered by direct measurements. Direct studies have been made on *planar* LEC with different luminescent polymers and electrolytes, with varying results depending on experimental conditions and selected material systems.[53, 74, 75]

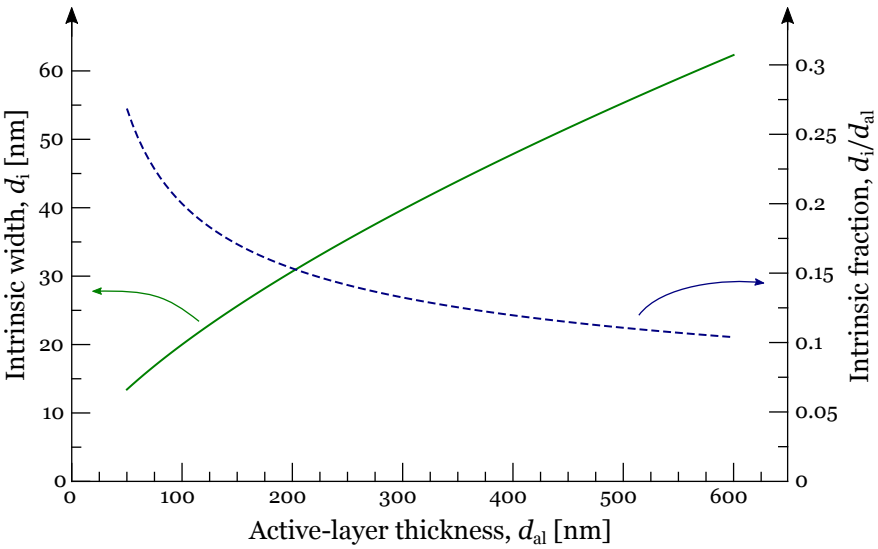

Figure 5.4: The modelled width of the intrinsic layer (solid green line), and the intrinsic width fraction of the active layer (dashed blue line), as a function of the active-layer thickness.

is fully doped and the operating voltage has reached its minimum value (during constant-current driving).[35] A constant gradient is an easy-to-understand and physically sensible doping profile, but it must be carefully implemented; our employed simulation software does not allow refractive-index gradients, but works only with discrete layers. We therefore discretize the transport regions and divide them into multiple layers with a stepwise decreasing doping concentration towards the intrinsic region, see black solid line and the inset in Fig. 5.5a.

To the second question there is no simple and general answer. Previous indirect studies of the intrinsic region width (d_i) on similar devices have employed e.g. impedance spectroscopy and drift-diffusion simulations, and report intrinsic width fractions (d_i/d_{al}) between 7 and 26 %.[35, 76] As d_i likely depend on the initial salt concentration, large variations are expected, and the values cannot be directly transferred across different material systems.[50] To get a representative steady-state d_i as a function of d_{al} for our investigated LECs, we instead turn to the electrical characterization. The straight fitted line of the operating voltage V_{op} versus d_{al} in Fig. 5.1 cuts the voltage-axis at ~2.7 V. This is close to the E_g of Super Yellow divided by the elementary charge, e (see distance between dashed lines in Fig. 4.2a), which indicates that the voltage drop at the active-layer|electrode interfaces is similar.[77] If we assume a negligible voltage drop over the doped transport regions with high conductivity, the drop

across the intrinsic region becomes $V_\mathrm{i} = V_\mathrm{op} - E_g/e$.[76] Electronic transport in undoped organic semiconductors can be expected to be space-charge limited rather than ohmic, so that the current density through an intrinsic layer depends on the square of the potential difference instead of being linear, according to Eq. (5.1). k is a constant that depends on e.g., the electronic properties of the material and the recombination rate of the charges, but this is not known for our devices.[78] So, based on the assumption that the exciton-diffusion distance is about 10 nm in organic semiconductors, we contend that the width of the intrinsic region for our best-performing LEC ($d_\mathrm{al} = 100$ nm) is 20 nm.[55, 59, 79] From these assumptions, and the relation between the steady-state operating voltage and the active-layer thickness displayed in Fig. 5.1b, we obtain a space-charge limited current model for how d_i depends on d_al at steady state in our investigated LECs. The result of this modelling is shown in Fig. 5.4, where we can see that d_i increases with d_al, but that $d_\mathrm{i}/d_\mathrm{al}$ decreases—from 26.9 % at $d_\mathrm{al} = 50$ nm to 10.4 % at $d_\mathrm{al} = 600$ nm.

$$J = k\frac{V_\mathrm{i}^2}{d_\mathrm{i}^3} \tag{5.1}$$

This leaves only the third question to complete the optical profile. While the naive choice would be to centre the intrinsic region in the active layer, we have seen that the optical response to doping of Super Yellow is asymmetric, and possibly other properties are as well; the position of the intrinsic region *is* an unknown parameter. Its effect on the doping profile is visualized in Fig. 5.5a, where a shift of the intrinsic region away from the centre towards any of electrodes implies strong changes to the doping-concentration levels and gradients. The related changes to the profiles of the refractive index and extinction coefficient are presented at $\lambda = 550$ nm in Fig. 5.5b and c, respectively.

To simulate emission from a device, the software models the excitons as oscillating dipoles that emits electromagnetic radiation, i.e. light. One of the required assumptions of this formalism is that the close surrounding of the dipoles is *strictly* transparent, so that $\kappa = 0$ and n' is real.[80] By positioning the dipoles in the intrinsic region that bridges the p- and n-type doped transport regions, it is possible to fulfil this criterion and retain non-zero absorption in the transport regions. As non-doped Super Yellow is virtually transparent in the emission range, we can define the extinction coefficient in the intrinsic layer to zero in the software, and expect it to be a good approximation. Also, keeping the emitting dipoles within the intrinsic region is in reasonable agreement with the electronic operation model described in chapter 2.

This opens up for an obvious relation between the optical profile of the active layer and the position and distribution of the emitting dipoles. We (admittedly somewhat arbitrarily) position all emitting dipoles precisely in the centre of the intrinsic region (i.e. with a δ-function distribution) and can thus state that

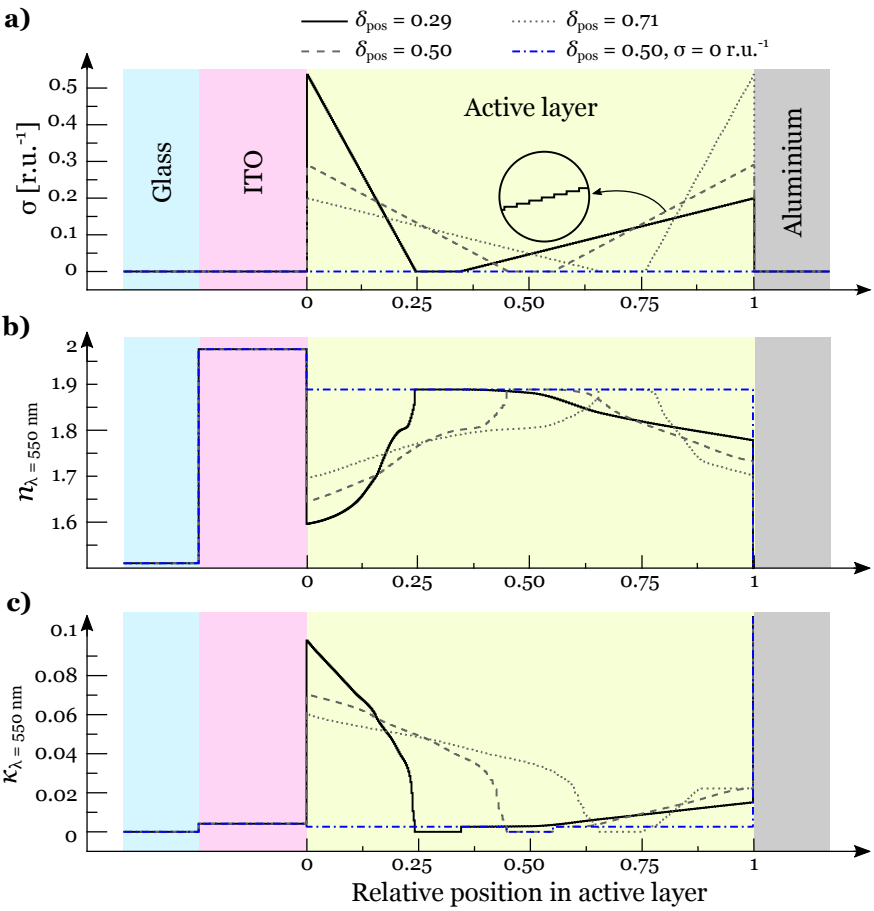

Figure 5.5: Profiles of the active layer. **a)** The doping concentration, **b)** the refractive index at 550 nm, which corresponds to the peak of the photoluminescence spectrum of Super Yellow, and **c)** the extinction coefficient at 550 nm. The profiles are drawn for an active-layer thickness of 600 nm, an average doping concentration of 0.13 r.u.$^{-1}$, and 100 sublayers in each transport region. δ_{pos} denotes the centre position of the intrinsic region.

the centre-position of the emitting dipole distribution and the intrinsic region coincide, and are *both* equal to δ_{pos}. Given a recombination current the optical simulation model can now be tested for different dipole positions and thicknesses of the active layer, with a parametrized optical profile for each case. However, the parametrization limits the possible positions of the emitting dipoles to between 0.265 and 0.735 of d_{al} away from the anode. At more extreme positions the required maximum local doping concentration exceeds the range of values for which the n' of Super Yellow can be reliably accessed, even through extrapolation of the measured values.[xiii] In a discretization test we find that the simulation set-up is surprisingly sensitive to the number of employed layers for each doped transport region. To avoid artefacts and maintain a reasonable computational cost, we therefore decide that an relative luminance error of less than 1 % is acceptable, which for our simulations requires at least 200 layers for each doped transport region.

5.3 Match between experiment and simulation

Since the LECs were investigated by a spectroscopic goniophotometer, we have access to the experimental viewing-angle dependent emission spectra $\left(I_e(\theta,\lambda)\right)$ for different thicknesses of the active layer. $I_e(\theta,\lambda)$ is highly sensitive to the position of the emitting dipoles, and this kind of emission-zone fit have been extensively used in research on organic light-emitting diodes, and recently to cyanine-based LECs.[81, 82] However, these studies employed a fixed optical profile of the devices, without taking doping-dependent optical properties into account. We have parametrized the doping profile and optical properties by linking the centre of the intrinsic region to the position of the emitting dipoles. This parametrization adds an extra layer of complexity to the simulation, for better and for worse.

To exclude thickness-dependent intensity variations from the fit of the emitter position, we scale $I_e(\theta,\lambda)$ for each thickness of the active layer by normalizing the spectrum in the forward direction, and maintaining the relative intensity change with viewing angle. We then set up a numerical routine that finds the best fit of δ_{pos} for each thickness. The routine minimizes the difference between the simulated and experimental angle-dependent emission spectra in terms of the mean absolute error ($\Delta I_{\lambda,\theta}$) as defined in Eq. (5.2), where $N_{\theta,\lambda} = N_\lambda N_\theta$ is the total number of comparison points.

$$\Delta I_{\lambda,\theta} = \sum_{\theta}\left(\sum_{\lambda}\left|I^{exp}_{\lambda,\theta}(\delta_{\text{pos}}) - I^{sim}_{\lambda,\theta}(\delta_{\text{pos}})\right|\right)\Big/ N_{\theta,\lambda} \tag{5.2}$$

[xiii] For example, at the δ_{pos} limits a 50 nm thick device has a maximum p- or n-type doping concentration of about 1 r.u.$^{-1}$, which is much larger than the measured maximum values of 0.2 and 0.6. Thus, to be able to implement a constant gradient doping profile we have extrapolated the measured n'-values from paper **III**, as shown in Fig. 4.3.

The error landscapes of the fits are presented in Fig. 5.6. All investigated thicknesses share a best fit of the emitter position of about 0.3, with the mean and standard deviation being 0.29(2). Thus, the relative emitter position is within the measured thickness range unaffected by the thickness of the active layer. To get a more tangible feeling for the quality of the fits, the experimental and simulated emission spectra for $\delta_{\text{pos}} = 0.29$ are shown in Fig. 5.7. The spectral fits are not perfect (and the $\Delta I_{\lambda,\theta}$ minima *are* non-zero) but must still be considered very good. We also looked at the emission spectra for emitter positions of 0.50 and 0.71. They qualitatively showed very bad correspondence between experiment and simulation, as directly reflected in the high $\Delta I_{\lambda,\theta}$. The flat $\Delta I_{\lambda,\theta}$ profiles of the best performing thin devices in Fig. 5.6 indicate that high performance devices could be ill suited for probing of device characteristics using spectral methods. However, the worst LECs from a performance point of view have deep and distinct minima. Since the relative emitter position is unchanged by the thickness of the active layer, and devices with different active-layer thickness thereby can be expected to have a qualitatively similar internal structure, such optically "detuned" devices can be used when trying to optimize new LEC architectures and material systems in the future.

After determining the emitter position, and thereby the position of the intrinsic region and the whole optical profile of the device, we moved on to simulate the forward luminance as a function of d_{al}. Overall the simulated results presented in Fig. 5.8 correspond well with the experimental luminance values,

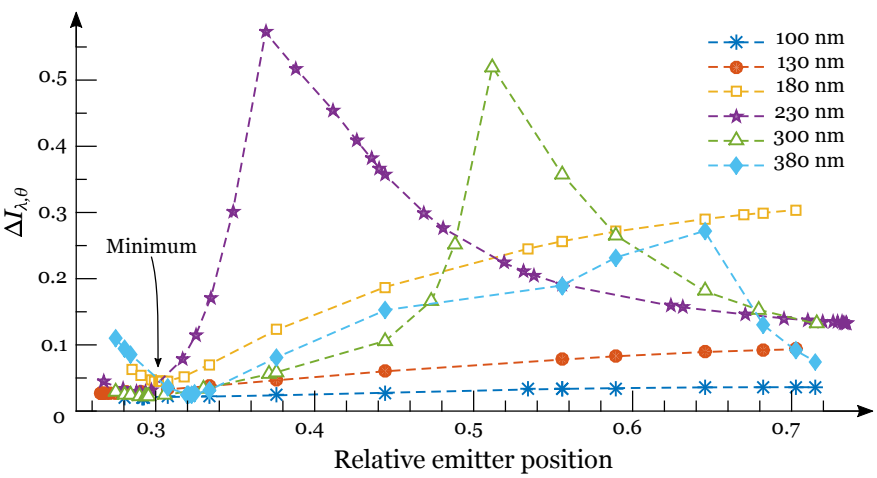

Figure 5.6: Error landscapes of the δ_{pos}-fits. The mean absolute error of the difference between the experimental and simulated emission spectra as a function of the emitting dipole position at different active-layer thicknesses.

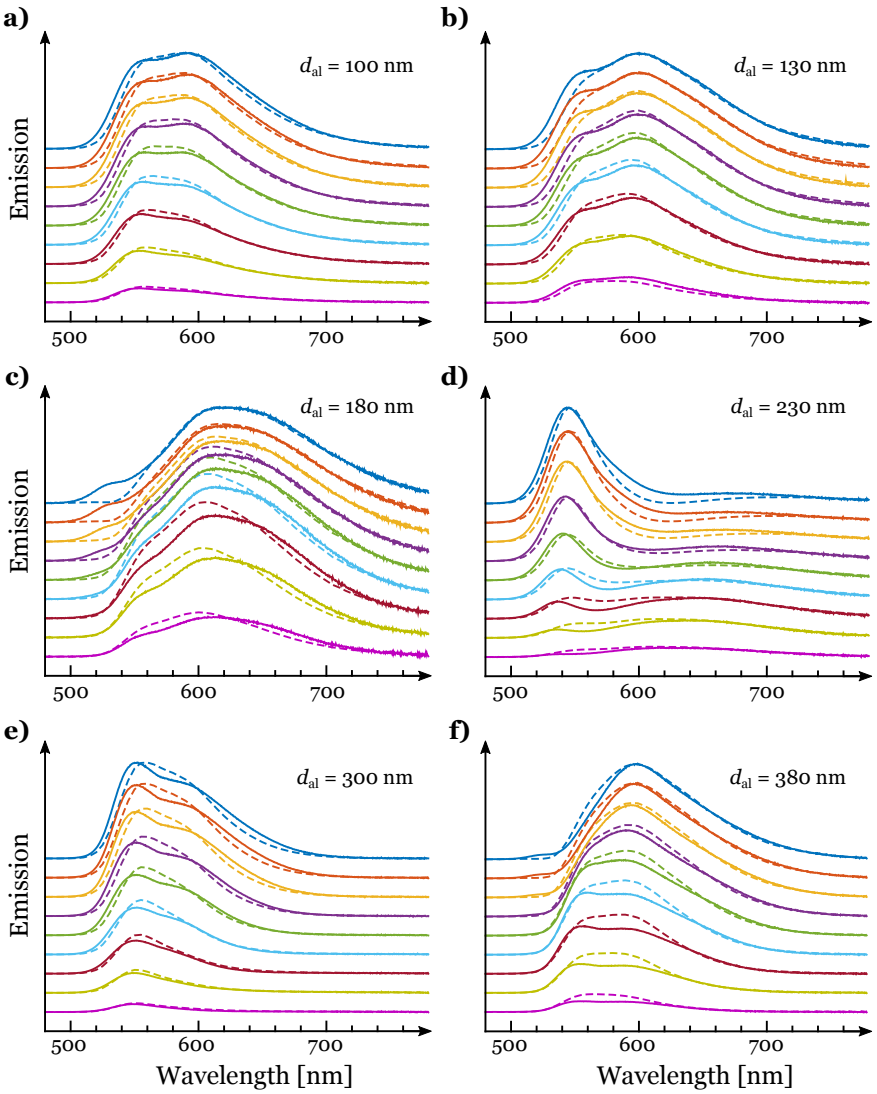

Figure 5.7: Experimental and simulated emission spectra. **a**-**f**) Stacked normalized angle-dependent emission spectra for active-layer thickness ranging from 100 to 380 nm. The viewing angles span 10 – 80° in steps of 10° degrees from the top to the bottom trace. The experimental spectra are shown as solid lines and the simulated spectra as dashed lines. The position of the emitting dipoles was set to 0.29 in the simulations.

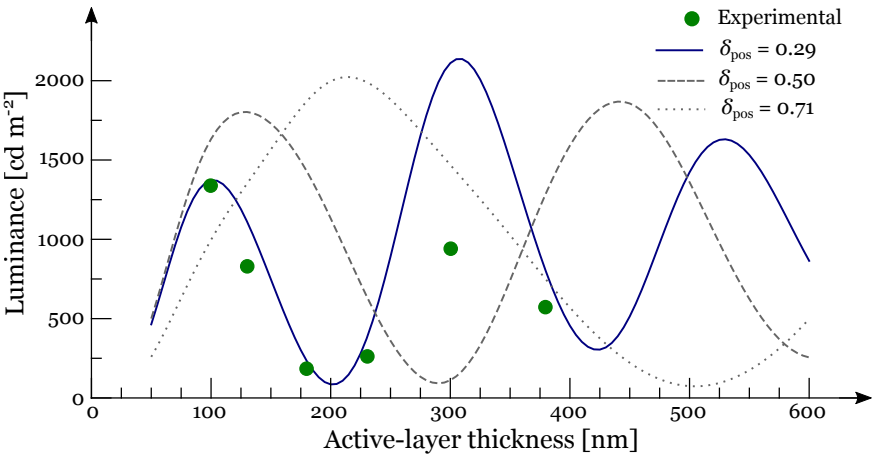

Figure 5.8: The forward luminance as a function of active-layer thickness. The experimental luminance is denoted by green solid circles, and the simulated luminance values are shown for an emitter position of 0.29 (blue solid line), 0.50 (grey dashed line), and 0.71 (grey dotted line).

both qualitatively and quantitatively. I especially want to point out that the periodicity of the experimental luminance is captured by this simulation model, given that we use the fitted $\delta_{pos} = 0.29$. Simulations for δ_{pos} of 0.50 and 0.71 show that the period of the luminance is sensitive to the simulated δ_{pos}. I am pleased with the results from this more complicated doping-dependent and coherent optical model and the progress that we have made. However, the model overestimates the luminance at the second order maximum, and at this stage we do not know the reason behind this discrepancy. If I allow myself to speculate, my guess is that the overestimation originates in a too simple description of the distribution of the emitting dipoles. This could result in an erroneous simulated number of excitons that decay in the intrinsic (and emissive) layer at a given current density. Given the pin-structure of an LEC, a unit recombination efficiency of holes and electrons is likely a good approximation, but if the recombination profile is broadened compared to our assumed δ-function, some of the charges are likely to recombine in the doped transport layers that we have modelled as non-emissive. Possibly, the overestimation could also result from non-flat interfaces, or an unknown degree of anisotropy and induced scattering in the thick and heavily doped transport regions, neither of which are accounted for in these simulations.

5.3.1 Sensitivity to the doping concentration

The simulations have up to now used the experimental average doping concentration (σ) of 0.13 r.u.$^{-1}$. However, by changing the average doping concentration in the simulations we can test the robustness to this parameter selection. The relation between the intrinsic and active-layer thicknesses is expected to change with the doping concentration in the device; but since the goal of these sensitivity simulations is not to replicate different experimental settings, we have kept the experimentally derived relation presented in Fig. 5.4 throughout.[50] Interestingly, even at σ = 0 r.u.$^{-1}$, fits of the emitter position give very similar results compared to those at a realistic doping concentration: the mean and standard deviation of the best fitted emitter positions is 0.320(8). The similarity between δ_{pos} = 0.29(2) for realistic doping, and δ_{pos} = 0.320(8) for zero doping, means that our method of extracting the position of the emitting dipoles is robust towards the employed doping profile and concentration. This is an important result because it implies that both parameters can be disregarded in simulations used for its extraction. The analysis becomes considerably simplified, and it adds credibility to previous studies that have used this method without taking a doping profile into account.[82]

If the goal of a simulation is to replicate or predict the luminous output of a device, the requirements are different. The simulated luminance is *highly* sensitive to the employed average doping concentration and profile, as shown in Fig. 5.9. The first and third order luminance maxima (at active-layer thicknesses of approximately 100 and 550 nm, respectively) are both strongly affected by a

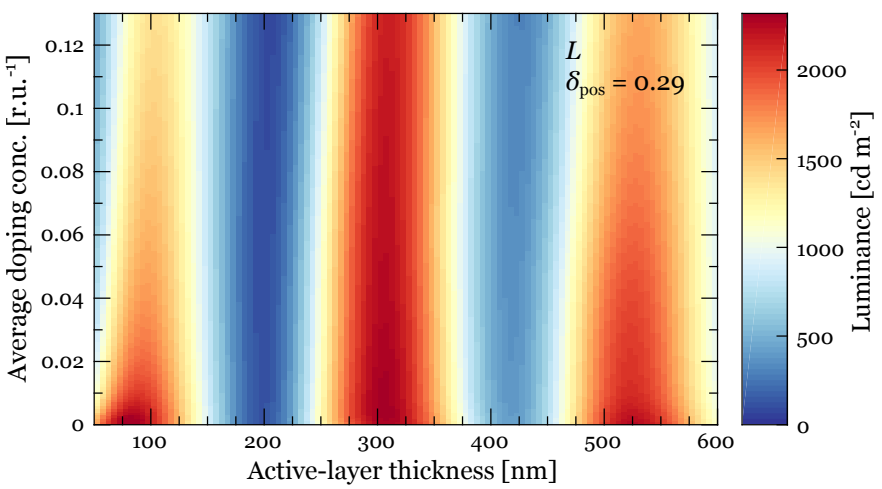

Figure 5.9: The simulated luminance as a function of average doping concentration (vertical axis) and active-layer thickness (horizontal axis).

shifted average doping concentration.[xiv] In general, a too low employed average doping concentration would bring an overestimation of the luminance. Optical simulations of LECs that aspire to quantify the emitted intensity *must* therefore employ a suitable doping profile and concentration.

5.4 Towards dynamic simulations

Our optical model is based on assumptions for the steady-state conditions of LECs, and extending the analysis to also capture the dynamic processes in LECs is complicated.[xv] We do not know what the doping profile looks like in the active layer during turn-on, and our steady-state results indicate that it is an important parameter for credible simulations. Experimental studies on the ion-distribution hint towards a non-trivial profile situation that depends on the initial ion concentration, operating conditions, and thickness of the active layer.[83] The measured ion profile does not necessarily reflect the doping concentration before an equilibrium at steady-state is reached, and the initial ion concentration profile in LECs can be inhomogeneous, which obstructs time-dependent electrical modelling of the doping profile because of non-trivial initial conditions.[84]

I am convinced that coupled electro-optical simulations, in which the evolution of the electrochemical doping and electronic charge-recombination profiles are directly connected to a doping-dependent optical simulation model, will eventually be able to accurately describe and predict the dynamic ionic and optoelectronic processes in LECs. Until we get there though, it can perhaps provoke some interest that some dynamic device parameters could be accessible by simpler means. Do you remember that we found the extraction of the (centre of the) emitter position in section 5.3.1 to be insensitive to the employed doping profile? For example, since our experimental device characterization is time resolved we should be able to track if and how the emitter position shifts during operation, disconnected from the doping evolution. In paper **IV** we experimentally found strong temporal changes to both the forward emission spectrum and the viewing-angle dependent luminous intensity.[82, 85, 86] I have no doubt that these changes were primarily caused by a shifting emitter position during the turn-on of the device. Given the existing data and our implemented optical model, this is a straightforward study, albeit pending, that would give a welcome contribution to the understanding of the dynamic processes in LECs.

[xiv] Interestingly, the second order maximum at ~300 nm appear more or less insensitive to the employed doping concentration. I will return to this observation in chapter 6.

[xv] If you feel tempted to interpret the doping-concentration axis in Fig. 5.9 as a rescaled time axis, there are number of reasons not to. For example, the steady-state luminance trend at $d_{\mathrm{al}} = 100$ nm decreases with doping, and we know that the experimental luminance for that thickness increases with time, see Fig. 5.2a.

6. Optical modes and loss channels

WE NOW HAVE AN OPTICAL MODEL of Super-Yellow based LECs that is implemented in a thin-film optical simulation framework. It reliably reproduces the experimental luminance, and viewing-angle dependent emission spectra and intensity. In order to learn more about the optical operation of our investigated LECs we can dissect the model and look at how different loss contributions are distributed in the simulations. I have already mentioned that propagating light can be absorbed by layers surrounding the excitons, and it is easy to understand that light with an emission angle larger than the critical angle for total internal reflection will be trapped in the glass substrate because of the refractive-index difference between glass and air. But can we expect more optical loss channels? How do they vary with the thickness of the active layer? And which are the most important losses to target in order to improve the efficiency of the devices?

6.1 Distribution of optical modes

The simulation software conveniently allows for an analysis of the different optical modes of the emission. In brief, the simulated emission is categorized based on its direction and intensity (the in-plane wave-vector) into seven different optical "modes" that are described below:

I_{nr}: The non-radiative intensity losses are caused by the fact that some excitons instead of emitting light funnel the excess energy into heat.

I_{ev}: The evanescent intensity consists of losses through the non-propagating part of the emission: to near-field absorption and surface-plasmon polaritons.

I_{wg}: The wave-guided mode intensity losses are caused by the fact that parts of the emission are trapped in the organic and semi-transparent electrode layers, and eventually absorbed.

I_{abs}: The absorbed intensity corresponds to losses to parasitic Beer-Lambert-like absorption in the device structure.

I_{btm}: The bottom intensity corresponds to the intensity that escapes the structure in the backward hemisphere. This could be considered a loss in some cases, and not in other. Because of the non-transmissive nature of the reflective aluminium cathode in our devices, I_{btm} is effectively zero.

I_{sub}: The substrate-bound intensity corresponds to the intensity that is lost because it is trapped in the substrate (glass for the herein presented devices).

I_{out}: The outcoupled intensity corresponds to the intensity that escapes the structure in the forward hemisphere. It is the useful and directly visible part of the emission.

The I_{nr} is to a first approximation described by one minus the photoluminescence quantum yield (PLQY) of the emitting material.[xvi] However, the optical cavity and structure can affect the radiative decay rate of the excitons so that the I_{nr} decreases. This is called the "Purcell"-effect and is commonly associated with a very efficient transfer to evanescently coupled modes.[87, 88] Since the power dissipated in the evanescent modes is non-emissive, the decrease of I_{nr} does generally not enhance the luminous output of a device.

The near-field absorption component in I_{ev} can be described as absorption caused by the evanescent and non-propagating electromagnetic field that surrounds an oscillating dipole. The intensity of this near-field scales with distance, r, from the emitting dipole and is $\propto 1/r^3$. In comparison, the propagating far-field intensity is $\propto 1/r$ and corresponds to Beer-Lambert absorption.[80] The surface-plasmon polariton component can be seen as charge-density oscillations that travel along organic-metal interfaces and are also induced by the near-field of the emitting dipoles.[87, 88]

Fig. 6.1 presents the distribution of the different optical modes in LECs as a function of d_{al}. I_{nr} is reduced for thin active layers as a result of the Purcell effect, in comparison to the value of unaffected $I_{nr} = 0.4$ at thicker active layers. The evanescent intensity constitutes the main loss channel for LECs with thin active layers. Although I_{ev} contains contributions from near-field absorption in the semitransparent ITO anode, and surface-plasmon polariton losses associated with the aluminium cathode, the length-scale dependence gives that it must be near-field absorption in the electrochemically doped transport regions that is the main culprit.[xvii]

We can also see that the losses to waveguiding in the active layer and ITO anode increases with d_{al}. Waveguiding is rarely discussed in the LEC field, but it is

[xvi] We have measured the PLQY of Super Yellow in thin film to be approximately 60 %, although we also saw that it is affected by the chemical composition of the film. Ions have a negative impact on the PLQY, whereas an ion-transporter dilutes the material and has positive impact. How this PLQY dependence should be implemented in a simulation, and how it would affect the results, remains to be investigated.

[xvii] This is supported by a simple comparison between the simulated I_{ev} in doped and non-doped LECs in paper **V**.

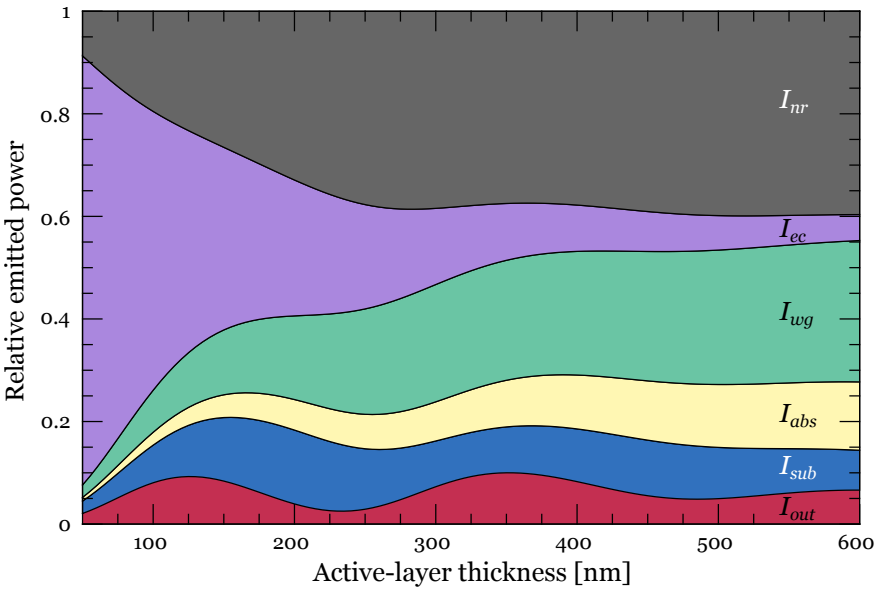

Figure 6.1: Simulation of the relative contributions (in unit of power) of the different optical modes for LECs with a varying active-layer thicknesses and an average doping concentration of 0.13 r.u.$^{-1}$.

one of the main loss channels for devices with thick active layers. I_{abs} increases monotonically with thickness just as we would expect, whereas I_{sub} and I_{out} are both periodic with respect to d_{al}, in line with the luminance in Fig. 5.8. According to the simulation, self-absorption at the second order maximum amounts to 9 % for a Super-Yellow based LEC with a doping concentration of 0.13 r.u.$^{-1}$. It is a considerable loss, on par with the substrate-bound losses (13 %), but the waveguided losses are in fact bigger than the sum of the two (23 %).

The combined optical losses are large compared to the outcoupled intensity in our LECs, which explains why our devices show quite moderate efficiencies. Optically, LECs with both thin and thick active layers are expected to be negatively affected by the electrochemical doping in the transport regions: For thin active layers, doping-enhanced evanescently coupled losses limit the available amount of light, and for thick active layers, waveguiding and doping-induced self-absorption are the main culprits. External outcoupling structures such as micro-lens arrays and half-sphere lenses target the substrate-bound modes, and have been successfully used in LECs.[38, 89, 90] An interesting observation is that LECs that are designed to be used with an external outcoupling structure typically should be fabricated with a slightly thicker active layer than devices designed to be used without it. Our results also support efforts to extract

wave-guided modes, especially for devices with thick active layers. This can be done by incorporating internal structures on the nano scale that interact with the light and push the (wave-vector of the) light from the wave-guided modes into the substrate or outcoupled modes.[91–94]

6.1.1 What difference does the doping?

To investigate the optical effects of the doping concentration, we vary both the average doping concentration and the thickness of the active layer in a mode-analysis simulation, see Fig. 6.2. A pattern of the outcoupled intensity that is qualitatively similar to that of the luminance (see Fig. 5.9) emerges, but the max and min features are slightly shifted to thicker active layers, and the doping-induced losses for the second order maximum are more prominent. Qualitative differences between these two figures are to be expected, as the outcoupled intensity takes the whole forward hemisphere into account, while the luminance is a directional and eye-response weighted metric.

The doping dependence of the evanescent losses is instructively shown at the first order maximum in Fig. 6.2. A decreasing average doping concentration not only increases the maximum out-coupled intensity, but also shifts the thickness of the active layer at which this maximum occurs, from 105 to 125 nm, as indicated by a dashed line. This d_{al}-maximum shift is a result of the strong distance dependence of near-field absorption described above. According to the simulations, the second order maximum is less affected by doping than the first order maximum. This can be rationalized by that waveguiding and self-absorption not yet have become prominent at this thickness, while the evanescently coupled losses already have been largely reduced. The experimental luminance at 300 nm was overestimated, so it is important to be careful with quantitative conclusions at these thicknesses. But still, if this insensitivity to doping at a certain thickness would *qualitatively* transfer to real devices, it would mean that there is a sweet-spot thickness for LECs at which the doping-induced optical losses are minimized.

In total, the mode analysis tells us that from an optical perspective, electrochemical doping impacts the luminous output negatively; devices with thin active layers suffer from increased losses to evanescently coupled modes, and thick devices suffer from increased polaron-induced self-absorption in the transport layers. In reality, “LEC” structures with zero or too-low doping concentration will of course be practically useless, as electrochemical doping is required in efficient LECs from an electrical point of view: it decreases the resistance of the device, enables high current-density driving at low operating voltage, and allows for the use of air-stable electrodes with retained electronic injection and simple fabrication of a single active layer. For an optimized combined electro-optical performance of LECs, a trade-off between the optical drawbacks and the electrical benefits of doping is necessary. We also note that

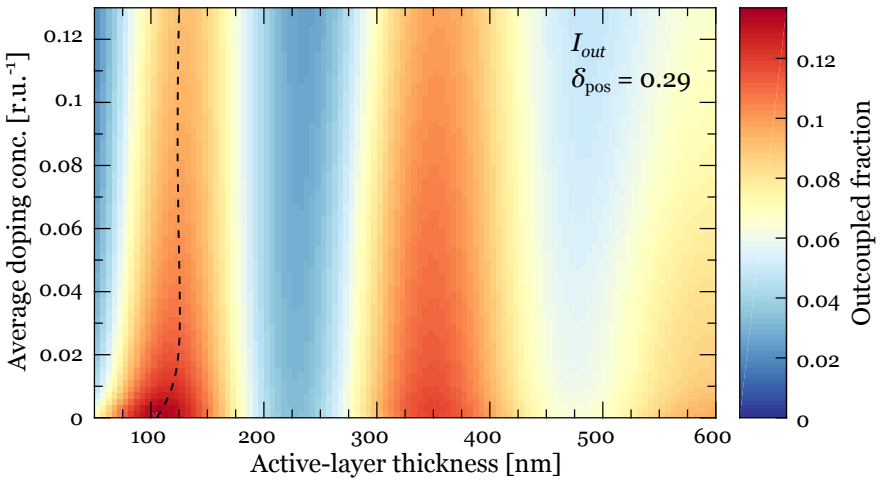

Figure 6.2: The simulated relative outcoupled intensity as a function of the active-layer thickness and average doping concentration.

the position of the emitters in general plays an important role, as it determines what active-layer thickness that give the luminous maxima, and thus which loss mechanisms that are dominant and need to be tackled. The LEC-field could benefit tremendously from employing many of the optical enhancement techniques that have already been developed for organic light-emitting diodes. At the same time, it is also painfully evident that the optical analysis of LECs is comparatively demanding, and requires a good understanding of the complex internal processes during operation.

6.2 Implicit particle-particle interactions?

I would like to take this opportunity to discuss a possible elephant in the room.[95] The simulation framework we use utilizes bulk material properties and classic electromagnetic field distributions, and as such it does not explicitly take particle-particle interactions into account, e.g., those between excitons and polarons.[80] As it has been firmly established that exciton-polaron quenching is a prominent hurdle for high-efficiency LECs, this limitation can be problematic. The effect of particle-particle interactions, like exciton-exciton and exciton-polaron quenching, are commonly computed using other simulation frameworks, e.g., kinetic Monte Carlo.[96] But, with four mobile charge carriers (electrons, holes, cation, and anions) and a dynamic evolution of the device structure, the simulations become involved and computationally expensive. To the best of my knowledge, no results from kinetic Monte

Carlo simulations on LECs have been published in the scientific literature. An interesting feature of the coupling to evanescent modes for doped LECs in Fig. 6.1b, is that its thickness dependence is similar to what we would expect from exciton-polaron quenching. The question is therefore what the difference between near-field absorption and exciton-polaron quenching really is, or if they effectively describe the same or overlapping processes, using different formalisms?

When we measure the doping-dependent refractive-index and extinction-coefficient spectra using the set-up described in chapter 4, we probe the light-matter interactions between the photons in the illumination beam and a doped Super-Yellow film (with a high density of polarons in the electrochemically doped state). We then extract the optical properties of the material that corresponds to these light-matter interactions—regardless of whether they are represented by waves and bulk materials, or as a sum of individual particle-particle interactions. Near-field absorption describes the absorption interaction between the evanescent electromagnetic field surrounding an oscillating dipole and a nearby absorbing bulk medium. Exciton-polaron quenching can on the other hand can be modelled as a Förster resonant energy transfer transition (*or* a charge-transfer transition corresponding to diffusion limited collisions between excitons and polarons).[49] In Förster resonant energy transfer, the transition matrix element describes the chance of energy transfer (quenching). As a result of the overlapping near-fields of two individual dipoles, rather than one dipole and one continuous medium, Förster resonant energy transfer is $\propto 1/r^6$.[97, 98] In terms of losses in LEC devices, we have not yet been able to distinguish the differences between near-field absorption in the electric-field and bulk-material picture, and exciton-polaron quenching in the particle picture.

To me, it seems plausible that the two descriptions are in fact different sides of the same coin. This would also explain how we could get such a good match between experimental and simulated forward luminance in Fig. 5.8. If exciton-polaron quenching was not implicitly accounted for in the evanescent modes, we would have expected the simulation to overestimate the luminance to "make room" for this additional loss channel.

7. Conclusions

IN THIS THESIS I ELABORATE ON THE OPTICAL OPERATION OF LECS. In papers **I** and **II** we conceive and fabricate bilayer LECs with separated electrolyte and luminescent polymer layers. The devices feature well-defined and adjustable patterned light emission in the form of pixels and line art. The resolution of the emissive patterns is given by the lateral spread of the ion-mediated electrochemical doping in the devices. We find that the lateral diffusion length of ions in pure Super Yellow is < 1 µm, which is below the resolution of the captured micrographs, but also a lateral growth of the emissive regions directed away from the electrolyte-free regions. We explain this growth by high hole conductivity of heavily p-doped Super Yellow that effectively works as an extension of the anode. Patterned bilayer LECs can possibly be applied in gadgets and security, but interestingly they also allow for a direct observation of doping-induced changes to the optical properties of the luminescent polymer film.

Super Yellow is a luminescent polymer that is often used in LECs, and its optical properties are strongly affected by electrochemical doping. In paper **III** we use a spectroelectrochemistry method to quantify the optical properties of Super Yellow in terms of the doping-dependent complex refractive-index spectra. During doping we find that the $\pi - \pi^\star$ transition of Super Yellow is bleached, which results in a lowered extinction coefficient (absorption) and refractive index in the short wavelength range. Concomitantly, the polarons bring an increase of the extinction coefficient and the refractive index in the red to near-infrared region. The effects of doping are asymmetric with respect to the doping type, with stronger bleaching and polaron absorption for hole-associated p-type doping than for electron-associated n-type doping. Doping-dependent refractive-index data are required for realistic optical simulations of LECs, and it is in that respect noteworthy that our study is the only source of such data for organic materials in the scientific domain.

In papers **IV** and **V** we investigate how the electroluminescent output of Super-Yellow based LECs is affected by changing the thickness of the active layer. From an electrical point of view, the differences are as expected small, but optically they are significant. The steady-state forward luminance (a standard

performance metric of LECs) decreases by approximately one order of magnitude following a thickness increase from 100 to 180 nm, and then partially recovers at 300 nm. This periodicity shows that an LEC model describing the optical operation should include coherent multilayer effects *and* the doping-dependent optical properties of Super Yellow from paper **III**. By parametrization of the doping profile and fitting of a single parameter (δ_{pos}) we can replicate the experimental luminous properties at steady state. We find that the relative position of the excitons in our Super-Yellow based sandwich LECs is independent of the thickness of the active layer and located ~30 % from the anode. This is qualitatively different from what is often observed in planar LECs, which points to the fingerspitzengefühl that is required for transferring properties between different device geometries and experimental conditions.

Our optical model predicts that thin LECs suffer from evanescently coupled losses to the electrochemically doped and absorbing transport regions, because of their close proximity to the emitting dipoles. Thick devices are also affected by an increasing doping concentration, but mainly through absorption of the propagating light. In addition to these two doping-induced effects, thick devices are limited by major structure-based losses to substrate-bound and wave-guided modes, which are both only weakly related to the doping concentration. Based on this distribution of optical losses, it is clear that optical design of the device structure is a necessity for the LEC technology to reach its full potential: If for example ITO was replaced by semi-transparent gold, the wave-guided losses would decrease, and inverting the structure to get top-emission could eliminate substrate-bound modes. For a given device structure, a carefully designed driving mode (that exploits the dynamic nature of the doped structure) can possibly be used to adjust the position of the excitons to an optimized location, or hold the intrinsic region in a dilated non-equilibrium state.

Perhaps the main contribution of this thesis lies in an enhanced optical understanding of LECs. Using patterned bilayer devices, we have visualized both the importance of electrochemical doping for light emission in LECs, and how high doping concentration can be too much of a good thing and result in quenched emission. I designed and built a new characterization set-up which we used to show the paramount importance of the thickness of the active layer for LECs with high luminous performance. We characterized the optical properties of Super Yellow in the electrochemically p- and n-doped state; thereby we could set up an optical model and replicate the measurements, which required that coherence and doping-concentration effects were considered. Our simulation results clarify the distribution of optical modes and losses in the devices, and how it might change with device thickness and doping concentration. These additions to the intricate optoelectric operation mechanism of LECs can direct and streamline future research, and take the field closer to real and useful new applications of light.

Contributions

Hereunder follows a brief specification of my contributions to each of the included papers.

I *Inkjet printed bilayer light-emitting electrochemical cells for display and lighting applications*

I performed all experimental work, collected and analysed the results, and actively participated in the writing of the manuscript.

II *Luminescent line art by direct-write patterning*

I performed all experimental work, collected and analysed the results, and actively participated in the writing of the manuscript.

III *On the asymmetric evolution of the optical properties of a conjugated polymer during electrochemical p- and n-type doping*

I designed and implemented the data-collection software. Together with the first author I designed the experimental measurement set-up and performed the experimental measurements. I did some of the data analysis and actively participated in the discussion and writing of the manuscript.

IV *The weak microcavity as an enabler for bright and fault-tolerant light-emitting electrochemical cells*

I designed the study, managed the project, built the measurement set-up, performed the experimental work and optical simulations, collected and analysed the results, and actively participated in writing the manuscript.

V *Optical analysis of light-emitting electrochemical cells*

I designed the study, managed the project, built the external simulation framework, performed the optical simulations, analysed the results, and actively participated in writing the manuscript.

Acknowledgements

"Never measure the height of a mountain until you reach the top. Then you will see how low it was." —Dag Hammarsköld

FIRST I WANT TO THANK MY FRIENDS AND FAMILY, and especially my wife, Marie. Without your patience, understanding, support, and sacrifices, I would not have been able to write this thesis—I am sorry about the intense finish.

I also want to thank my main supervisor Ludvig Edman, for accepting me as a PhD student, and for letting me do challenging research that I find meaningful and interesting. Further, it has been a privilege to work in the cool, free, and creative research and teaching environment that is the Physics Department in Umeå, with outstanding support from the technical and administrative personnel. I want to express appreciation of the many scientific and non-scientific discussions I have had with numerous colleagues and friends in OPEG, at IceLab, and in the fika room over the years. In particular, I have truly enjoyed the limited amount of coffee that I have consumed with Petter Lundberg, and the great perspectives on life and science that Thomas Lanz and Ludvig Bohlin so generously have shared with me. Also, Alexandra Johansson and Erik Wallin deserve some explicit credits for giving me a head start with LaTeX templates, so that I could comfortably get rid of a common WYSIWYG word processor.

Last, I want to seize this opportunity to thank *you* on behalf of the children of today and tomorrow: Thank you for daring to face the uncomfortable challenges of our time, and for acting *now* for a just transition towards a resilient and sustainable global human society.[99, 100] They are worth it.

Bibliography

1. Intergovernmental Panel on Climate Change. *Special Report: Global Warming of 1.5* °C (2018).
2. Ripple, W. J., Wolf, C., Newsome, T. M., Galetti, M., Alamgir, M., Crist, E., Mahmoud, M. I., Laurance, W. F. & 15364 scientist signatories from 184 countries. World Scientists' Warning to Humanity: A Second Notice. *BioScience* **67,** 1026–1028 (2017).
3. Figueres, C. & Thunberg, G. Op-ed: Davos, this is outrageous. *The Washington Post*. `https://www.washingtonpost.com/news/theworldpost/wp/2019/01/23/davos` (2019).
4. Rockström, J. *et al.* A safe operating space for humanity. *Nature* **461,** 472–475 (2009).
5. Steffen, W., Rockström, J., Richardson, K., Lenton, T. M., Folke, C., Liverman, D., Summerhayes, C. P., Barnosky, A. D., Cornell, S. E., Crucifix, M., Donges, J. F., Fetzer, I., Lade, S. J., Scheffer, M., Winkelmann, R. & Schellnhuber, H. J. Trajectories of the Earth System in the Anthropocene. *Proceedings of the National Academy of Sciences* **115,** 8252–8259 (2018).
6. Barnosky, A. D., Matzke, N., Tomiya, S., Wogan, G. O. U., Swartz, B., Quental, T. B., Marshall, C., McGuire, J. L., Lindsey, E. L., Maguire, K. C., Mersey, B. & Ferrer, E. A. Has the Earth's sixth mass extinction already arrived? *Nature* **471,** 51–57 (2011).
7. Barboza, L. G. A., Vethaak, A. D., Lavorante, B. R., Lundebye, A. K. & Guilhermino, L. Marine microplastic debris: An emerging issue for food security, food safety and human health. *Marine Pollution Bulletin* **133,** 336–348 (2018).
8. Haward, M. Plastic pollution of the world's seas and oceans as a contemporary challenge in ocean governance. *Nature Communications* **9,** 667 (2018).

9. Brodin, T., Fick, J., Jonsson, M. & Klaminder, J. Dilute Concentrations of a Psychiatric Drug Alter Behavior of Fish from Natural Populations. *Science* **339,** 814–815 (2013).
10. Demselben. Ueber den flüssigen Storax (Styrax liquidus). *Annalen der Pharmazie* **31,** 265–277 (1839).
11. Baumann, E. Ueber einige Vinylverbindungen. *Annalen der Chemie und Pharmacie* **163,** 308–322 (1872).
12. Von Pechmann, H. Ueber Diazomethan und Nitrosoacylamine. *Berichte der Deutschen Chemischen Gesellschaft* **31,** 2640–2646 (1898).
13. Shirakawa, H., Louis, E. J., Macdiarmid, A. G., Chiang, C. K. & Heeger, A. J. Synthesis of Electrically Conducting Organic Polymers - Halogen Derivatives of Polyacetylene, $(CH)_X$. *Journal of the Chemical Society, Chemical Communications,* 578–580 (1977).
14. The Royal Swedish Academy of Sciences. *The Nobel Prize in Chemistry 2000: Advanced information* (2000).
15. Feast, W., Tsibouklis, J., Pouwer, K., Groenendaal, L. & Meijer, E. Synthesis, processing and material properties of conjugated polymers. *Polymer* **37,** 5017–5047 (1996).
16. Mele, G. & Epstein, A. Foreword - Celebrating the year 2000 Nobel Prize in Chemistry to Alan Heeger, Alan MacDiarmid and Hideki Shirakawa for the discovery and development of conductive polymers. *Synthetic Metals* **125,** 1 (2001).
17. Geoghegan, M. & Hadziiannou, G. *Polymer Electronics* ISBN: 9780199533824 (Oxford University Press, 2013).
18. Camurlu, P. Polypyrrole derivatives for electrochromic applications. *RSC Advances* **4,** 55832–55845 (2014).
19. Sariciftci, N. S., Smilowitz, L., Heeger, A. J. & Wudl, F. Photoinduced Electron-Transfer from a Conducting Polymer to Buckminsterfullerene. *Science* **258,** 1474–1476 (1992).
20. Burroughes, J. H., Bradley, D. D. C., Brown, A. R., Marks, R. N., Mackay, K., Friend, R. H., Burns, P. L. & Holmes, A. B. Light-Emitting-Diodes Based on Conjugated Polymers. *Nature* **347,** 539–541 (1990).
21. Liang, J. J., Li, L., Niu, X. F., Yu, Z. B. & Pei, Q. B. Elastomeric polymer light-emitting devices and displays. *Nature Photonics* **7,** 817–824 (2013).
22. Asadpoordarvish, A., Sandström, A., Larsen, C., Bollström, R., Toivakka, M., Österbacka, R. & Edman, L. Light-Emitting Paper. *Advanced Functional Materials* **25,** 3238–3245 (2015).

23. Zhang, Z. T., Guo, K. P., Li, Y. M., Li, X. Y., Guan, G. Z., Li, H. P., Luo, Y. F., Zhao, F. Y., Zhang, Q., Wei, B., Pei, Q. B. & Peng, H. S. A colour-tunable, weavable fibre-shaped polymer light-emitting electrochemical cell. *Nature Photonics* **9,** 233–238 (2015).

24. Lanz, T., Sandström, A., Tang, S., Chabrecek, P., Sonderegger, U. & Edman, L. A light–emission textile device: conformal spray-sintering of a woven fabric electrode. *Flexible and Printed Electronics* **1,** 025004 (2016).

25. Mauthner, G., Landfester, K., Kock, A., Bruckl, H., Kast, M., Stepper, C. & List, E. J. Inkjet printed surface cell light-emitting devices from a water-based polymer dispersion. *Organic Electronics* **9,** 164–170 (2008).

26. Sandström, A., Dam, H. F., Krebs, F. C. & Edman, L. Ambient fabrication of flexible and large-area organic light-emitting devices using slot-die coating. *Nature Communications* **3,** 1002 (2012).

27. Liang, J. J., Li, L., Niu, X. F., Yu, Z. B. & Pei, Q. B. Fully Solution-Based Fabrication of Flexible Light-Emitting Device at Ambient Conditions. *Journal of Physical Chemistry C* **117,** 16632–16639 (2013).

28. Hernandez-Sosa, G., Tekoglu, S., Stolz, S., Eckstein, R., Teusch, C., Trapp, J., Lemmer, U., Hamburger, M. & Mechau, N. The Compromises of Printing Organic Electronics: A Case Study of Gravure-Printed Light-Emitting Electrochemical Cells. *Advanced Materials,* 3235–3240 (2014).

29. Sandström, A. & Edman, L. Towards High-Throughput Coating and Printing of Light-Emitting Electrochemical Cells: A Review and Cost Analysis of Current and Future Methods. *Energy Technology* **3,** 329–339 (2015).

30. Zimmermann, J., Schlisske, S., Held, M., Tisserant, J. N., Porcarelli, L., Sanchez-Sanchez, A., Mecerreyes, D. & Hernandez-Sosa, G. Ultrathin Fully Printed Light-Emitting Electrochemical Cells with Arbitrary Designs on Biocompatible Substrates. *Advanced Materials Technologies,* 1800641 (2019).

31. Pei, Q. B., Yu, G., Zhang, C., Yang, Y. & Heeger, A. J. Polymer Light-Emitting Electrochemical-Cells. *Science* **269,** 1086–1088 (1995).

32. Pei, Q. B., Yang, Y., Yu, G., Zhang, C. & Heeger, A. J. Polymer light-emitting electrochemical cells: In situ formation of a light-emitting p-n junction. *Journal of the American Chemical Society* **118,** 3922–3929 (1996).

33. Smith, D. L. Steady state model for polymer light-emitting electrochemical cells. *Journal of Applied Physics* **81,** 2869–2880 (1997).

34. deMello, J. C. Interfacial feedback dynamics in polymer light-emitting electrochemical cells. *Physical Review B* **66,** 235210 (2002).

35. Van Reenen, S., Matyba, P., Dzwilewski, A., Janssen, R. A. J., Edman, L. & Kemerink, M. A Unifying Model for the Operation of Light-Emitting Electrochemical Cells. *Journal of the American Chemical Society* **132,** 13776–13781 (2010).

36. Matyba, P., Yamaguchi, H., Eda, G., Chhowalla, M., Edman, L. & Robinson, N. D. Graphene and Mobile Ions: The Key to All-Plastic, Solution-Processed Light-Emitting Devices. *ACS Nano* **4,** 637–642 (2010).

37. Lundberg, P., Lindh, E. M., Tang, S. & Edman, L. Toward Efficient and Metal-Free Emissive Devices: A Solution Processed Host Guest Light-Emitting Electrochemical Cell Featuring Thermally Activated Delayed Fluorescence. *ACS Applied Materials & Interfaces* **9,** 28810–28816 (2017).

38. Tang, S., Sandström, A., Lundberg, P., Lanz, T., Larsen, C., van Reenen, S., Kemerink, M. & Edman, L. Design rules for light-emitting electrochemical cells delivering bright luminance at 27.5 percent external quantum efficiency. *Nature Communications* **8,** 1190 (2017).

39. Su, H. C. Optical Techniques for Light-Emitting Electrochemical Cells. *ChemPlusChem* **83,** 197–210 (2018).

40. Jenatsch, S., Wang, L., Bulloni, M., Veron, A. C., Ruhstaller, B., Altazin, S., Nuesch, F. & Hany, R. Doping Evolution and Junction Formation in Stacked Cyanine Dye Light-Emitting Electrochemical Cells. *ACS Applied Materials & Interfaces* **8,** 6554–6562 (2016).

41. Diethelm, M., Grossmann, Q., Schiller, A., Knapp, E., Jenatsch, S., Kawecki, M., Nüesch, F. & Hany, R. Optimized Electrolyte Loading and Active Film Thickness for Sandwich Polymer Light-Emitting Electrochemical Cells. *Advanced Optical Materials,* 1801278 (2018).

42. Coelho, P. *Manual of the warrior of light* ISBN: 0007156324 (HarperCollins Publishers, 2002).

43. Samuel, J. & Edwars, P. *Solvent-Based Inkjet Inks* (ed Magdassi, S) chap. 8. ISBN: 109812818219 (World Scientific Publishing, 2010).

44. McPeak, K. M., Jayanti, S. V., Kress, S. J. P., Meyer, S., Iotti, S., Rossinelli, A. & Norris, D. J. Plasmonic Films Can Easily Be Better: Rules and Recipes. *ACS Photonics* **2,** 326–333 (2015).

45. Fox, M. *Optical Properties of Solids* 2nd. ISBN: 9780199573370 (Oxford University Press, 2010).

46. deMello, J. C., Tessler, N., Graham, S. C. & Friend, R. H. Ionic space-charge effects in polymer light-emitting diodes. *Physical Review B* **57,** 12951–12963 (1998).

47. Pei, Q. & Heeger, A. J. Operating mechanism of light-emitting electrochemical cells. *Nature Materials* **7,** 167–167 (2008).

48. Ashcroft, N. W. & Mermin, N. D. *Solid State Physics* ISBN: 9780030839931 (Cengage Learning, 1976).

49. Van Reenen, S., Vitorino, M. V., Meskers, S. C. J., Janssen, R. A. J. & Kemerink, M. Photoluminescence quenching in films of conjugated polymers by electrochemical doping. *Physical Review B* **89,** 205206 (2014).

50. Van Reenen, S., Matyba, P., Dzwilewski, A., Janssen, R. A. J., Edman, L. & Kemerink, M. Salt Concentration Effects in Planar Light-Emitting Electrochemical Cells. *Advanced Functional Materials* **21,** 1795–1802 (2011).

51. Van Reenen, S., Janssen, R. A. J. & Kemerink, M. Fundamental Tradeoff between Emission Intensity and Efficiency in Light-Emitting Electrochemical Cells. *Advanced Functional Materials* **25,** 3066–3073 (2015).

52. Matyba, P., Maturova, K., Kemerink, M., Robinson, N. D. & Edman, L. The dynamic organic p-n junction. *Nature Materials* **8,** 672–676 (2009).

53. AlTal, F. & Gao, J. High resolution scanning optical imaging of a frozen polymer p-n junction. *Journal of Applied Physics* **120,** 115501 (2016).

54. Sandström, A., Matyba, P., Inganäs, O. & Edman, L. Separating Ion and Electron Transport: The Bilayer Light-Emitting Electrochemical Cell. *Journal of the American Chemical Society* **132,** 6646–6647 (2010).

55. Sandström, A., Matyba, P. & Edman, L. Yellow-green light-emitting electrochemical cells with long lifetime and high efficiency. *Applied Physics Letters* **96,** 053303 (2010).

56. Byrne, F. P., Jin, S., Paggiola, G., Petchey, T. H. M., Clark, J. H., Farmer, T. J., Hunt, A. J., Robert McElroy, C. & Sherwood, J. Tools and techniques for solvent selection: green solvent selection guides. *Sustainable Chemical Processes* **4,** 7 (2016).

57. Deegan, R. D., Bakajin, O., Dupont, T. F., Huber, G., Nagel, S. R. & Witten, T. A. Capillary flow as the cause of ring stains from dried liquid drops. *Nature* **389,** 827–829 (1997).

58. Shin, J. H., Robinson, N. D., Xiao, S. & Edman, L. Polymer light-emitting electrochemical cells: Doping concentration, emission-zone position, and turn-on time. *Advanced Functional Materials* **17,** 1807–1813 (2007).

59. Fang, J. F., Matyba, P. & Edman, L. The Design and Realization of Flexible, Long-Lived Light-Emitting Electrochemical Cells. *Advanced Functional Materials* **19,** 2671–2676 (2009).

60. Mortimer, R. J., Dyer, A. L. & Reynolds, J. R. Electrochromic organic and polymeric materials for display applications. *Displays* **27,** 2–18 (2006).

61. Campoy-Quiles, M., Alonso, M. I., Bradley, D. D. C. & Richter, L. J. Advanced Ellipsometric Characterization of Conjugated Polymer Films. *Advanced Functional Materials* **24,** 2116–2134 (2014).

62. Gruska, B. & Peters, S. *Organic Light Emitting Diodes (OLED's)* tech. rep. (Sentech Instruments GmbH).

63. Kaihovirta, N., Asadpoordarvish, A., Sandström, A. & Edman, L. Doping-Induced Self-Absorption in Light-Emitting Electrochemical Cells. *ACS Photonics* **1,** 182–189 (2014).

64. Holt, A. L., Leger, J. M. & Carter, S. A. Electrochemical and optical characterization of p- and n-doped poly[2-methoxy-5-(2-ethylhexyloxy)-1,4-phenylenevinylene]. *Journal of Chemical Physics* **123,** 044704 (2005).

65. Bröms, P., Fahlman, M., Xing, K. Z., Salaneck, W. R., Dannetun, P., Cornil, J., Dossantos, D. A., Bredas, J. L., Moratti, S. C., Holmes, A. B. & Friend, R. H. Optical-Absorption Studies of Sodium Doped poly(cyanoterephthalylidene). *Synthetic Metals* **67,** 93–96 (1994).

66. Cornil, J., Beljonne, D. & Bredas, J. L. Nature of Optical-Transitions in Conjugated Oligomers .1. Theoretical Characterization of Neutral and Doped oligo(phenylenevinylene)s. *Journal of Chemical Physics* **103,** 834–841 (1995).

67. Jafari, M. J., Liu, J., Engquist, I. & Ederth, T. Time-Resolved Chemical Mapping in Light-Emitting Electrochemical Cells. *ACS Applied Materials & Interfaces* **9,** 2747–2757 (2017).

68. Li, X. Y., Gao, J. & Liu, G. J. Thickness dependent device characteristics of sandwich polymer light-emitting electrochemical cell. *Organic Electronics* **14,** 1441–1446 (2013).

69. Jhang, Y. P., Chen, H. F., Wu, H. B., Yeh, Y. S., Su, H. C. & Wong, K. T. Improving device efficiencies of solid-state white light-emitting electrochemical cells by adjusting the emissive-layer thickness. *Organic Electronics* **14,** 2424–2430 (2013).

70. Gather, M. C. & Reineke, S. Recent advances in light outcoupling from white organic light-emitting diodes. *Journal of Photonics for Energy* **5,** 057607 (2015).

71. Cushman, C. V., Sturgell, B. A., Martin, A. C., Lunt, B. M., Smith, N. J. & Linford, M. R. Eagle XG® glass, optical constants from 230 to 1690 nm (0.73 - 5.39 eV) by spectroscopic ellipsometry. *Surface Science Spectra* **23,** 55–60 (2016).

72. Lanz, T., Lindh, E. M. & Edman, L. On the Asymmetric Evolution of the Optical Properties of a Conjugated Polymer during Electrochemical p- and n-type Doping. *Journal of Materials Chemistry C* **5,** 4706–4715 (2017).

73. Fang, J., Matyba, P., Robinson, N. D. & Edman, L. Identifying and alleviating electrochemical side-reactions in light-emitting electrochemical cells. *Journal of the American Chemical Society* **130,** 4562–4568 (2008).

74. Robinson, N. D., Fang, J. F., Matyba, P. & Edman, L. Electrochemical doping during light emission in polymer light-emitting electrochemical cells. *Physical Review B* **78,** 245202 (2008).

75. Matyba, P., Andersson, M. R. & Edman, L. On the desired properties of a conjugated polymer-electrolyte blend in a light-emitting electrochemical cell. *Organic Electronics* **9,** 699–710 (2008).

76. Munar, A., Sandstrom, A., Tang, S. & Edman, L. Shedding Light on the Operation of Polymer Light-Emitting Electrochemical Cells Using Impedance Spectroscopy. *Advanced Functional Materials* **22,** 1511–1517 (2012).

77. Xu, J., Sandström, A., Lindh, E. M., Yang, W., Tang, S. & Edman, L. Challenging Conventional Wisdom: Finding High-Performance Electrodes for Light-Emitting Electrochemical Cells. *ACS Applied Materials & Interfaces* **10,** 33380–33389 (2018).

78. Pope, M. & Swenberg, C. E. *Electronic Processes in Organic Crystals and Polymers* 2nd. ISBN: 9780195129632 (Oxford University Press, 1999).

79. Tamai, Y., Ohkita, H., Benten, H. & Ito, S. Exciton Diffusion in Conjugated Polymers: From Fundamental Understanding to Improvement in Photovoltaic Conversion Efficiency. *Journal of Physical Chemistry Letters* **6,** 3417–3428 (2015).

80. *setfos 4.6 User Manual* Fluxim AG (2018).

81. Perucco, B., Reinke, N. A., Rezzonico, D., Moos, M. & Ruhstaller, B. Analysis of the emission profile in organic light-emitting devices. *Optics Express* **18,** A246–A260 (2010).

82. Jenatsch, S., Regnat, M., Hany, R., Diethelm, M., Nuesch, F. & Ruhstaller, B. Time-Dependent p-i-n Structure and Emission Zone in Sandwich-Type Light-Emitting Electrochemical Cells. *ACS Photonics* **5,** 1591–1598 (2018).

83. Shoji, T. D., Zhu, Z. H. & Leger, J. M. Characterizing Ion Profiles in Dynamic Junction Light-Emitting Electrochemical Cells. *ACS Applied Materials & Interfaces* **5,** 11509–11514 (2013).

84. Kawecki, M., Hany, R., Diethelm, M., Jenatsch, S., Grossmann, Q., Bernard, L. & Josef Hug, H. Direct Measurement of Ion Redistribution and Resulting Modification of Chemical Equilibria in Polymer Thin Film Light-Emitting Electrochemical Cells. *ACS Applied Materials & Interfaces* **10,** 39100–39106 (2018).

85. Sun, R., Liao, C. T. & Su, H. C. Effects of incorporating salts with various alkyl chain lengths on carrier balance of light-emitting electrochemical cells. *Organic Electronics* **15,** 2885–2892 (2014).

86. Devižis, A., Jenatsch, S., Diethelm, M., Gulbinas, V., Nüesch, F. & Hany, R. Dynamics of Charge Distribution in Sandwich-Type Light-Emitting Electrochemical Cells Probed by the Stark Effect. *ACS Photonics* **5,** 3124–3131 (2018).

87. Barnes, W. L. Fluorescence near interfaces: The role of photonic mode density. *Journal of Modern Optics* **45,** 661–699 (1998).

88. Penninck, L., Mladenowski, S. & Neyts, K. The effects of planar metallic interfaces on the radiation of nearby electrical dipoles. *Journal of Optics* **12,** 075001 (2010).

89. Kaihovirta, N., Larsen, C. & Edman, L. Improving the Performance of Light-Emitting Electrochemical Cells by Optical Design. *ACS Applied Materials & Interfaces* **6,** 2940–2947 (2014).

90. Jang, Y. F., Lin, T. C., Guo, J. Y., Chiang, C. M., Wu, M. L., Shen, H. Y., Chen, T. C., Yang, Z. P., Lee, Y. J., Su, H. C., Chang, C. H. & Liu, S. W. Enhancing extracted electroluminescence from light-emitting electrochemical cells by employing high-refractive-index substrates. *Organic Electronics* (2017).

91. Ziebarth, J. M., Saafir, A. K., Fan, S. & McGehee, M. D. Extracting Light from Polymer Light-Emitting Diodes Using Stamped Bragg Gratings. *Advanced Functional Materials* **14,** 451–456 (2004).

92. Koo, W. H., Jeong, S. M., Araoka, F., Ishikawa, K., Nishimura, S., Toyooka, T. & Takezoe, H. Light extraction from organic light-emitting diodes enhanced by spontaneously formed buckles. *Nature Photonics* **4,** 222–226 (2010).

93. Koo, W. H., Youn, W., Zhu, P., Li, X. H., Tansu, N. & So, F. Light Extraction of Organic Light Emitting Diodes by Defective Hexagonal-Close-Packed Array. *Advanced Functional Materials* **22,** 3454–3459 (2012).

94. Sato, K., Uchida, S., Toriyama, S., Nishimura, S., Oyaizu, K., Nishide, H. & Nishikitani, Y. Low-Cost, Organic Light-Emitting Electrochemical Cells with Mass-Producible Nanoimprinted Substrates Made Using Roll-to-Roll Methods. *Advanced Materials Technologies* **2,** 1600293 (2017).

95. McComb, K., Moss, C., Durant, S. M., Baker, L. & Sayialel, S. Matriarchs as repositories of social knowledge in African elephants. *Science* **292,** 491–494 (2001).

96. Coehoorn, R., Zhang, L., Bobbert, P. A. & van Eersel, H. Effect of polaron diffusion on exciton-polaron quenching in disordered organic semiconductors. *Physical Review B* **95,** 134202 (2017).

97. Clegg, R. M. Förster resonance energy transfer–FRET what is it, why do it, and how it's done. *Laboratory Techniques in Biochemistry and Molecular Biology* **33,** 1–57 (2009).

98. Periasamy, A. & Day, R. N. *Molecular Imaging: FRET Microscopy and Spectroscopy* ISBN: 9780195177206 (Academic Press, 2008).

99. Klein, N. *This changes everything* ISBN: 9780241956182 (Penguin Books, 2015).

100. Robinson, M. & Shine, T. Achieving a climate justice pathway to 1.5 °C. *Nature Climate Change* **8,** 564–569 (2018).